



Prediction of the standardized precipitation index based on the long short-term memory and empirical mode decomposition-extreme learning machine models: The Case of Sakarya, Türkiye

Ömer Coşkun ^a, Hatice Citakoglu ^{b,*}

^a Turkish General Directorate of State Hydraulic Works (DSİ), Kayseri, Turkey

^b Department of Civil Engineering, Erciyes University, Kayseri, Turkey



ARTICLE INFO

Keywords:

Meteorological drought
Drought prediction
Standardized precipitation index (SPI)
Long short-term memory (LSTM)
Extreme learning machine (ELM)
Empirical mode decomposition (EMD)
Türkiye

ABSTRACT

This research predicted the meteorological drought of Sakarya province in northwest Türkiye using long short-term memory (LSTM). This deep learning algorithm has gained popularity in prediction studies. The standardized precipitation index (SPI), which can only be derived using precipitation data, was utilized for 1, 3, and 6-month time scales. SPI-1, SPI-3, and SPI-6-month time scales drought data calculated from the monthly precipitation data of the Sakarya Meteorology Station between 1960 and 2020 were taken as input data in the LSTM model. SPI drought data were used between 1960 and 2005 as training data and 2006–2020 as test data. Drought at $t+1$ output time was predicted using SPI values at t , $t-1$, $t-2$, and $t-3$ lag times as input variables. In addition, the results were compared with the empirical mode decomposition (EMD)-extreme learning machine (ELM) hybrid model to understand the capabilities of the standalone LSTM prediction model. The LSTM model yielded the best results ($MAE = 0.11$, $NSE = 0.97$, $R^2 = 0.97$) for the SPI-1-month time scale and the best results ($MAE = 0.18$, $NSE = 0.92$, $R^2 = 0.94$) for 3-month time scale. The EMD-ELM hybrid model yielded the best results ($MAE = 0.22$, $NSE = 0.95$, $R^2 = 0.96$) for the SPI-6-month time scale. Due to the high performance of this study's proposed standalone LSTM model, it was concluded that drought time series do not need to be subjected to pre-processing techniques.

1. Introduction

Many parts of the world are struggling with drought and the negativities it causes. It is linked to water availability, resulting in water shortage, stress associated with water management, agricultural productivity reduction, food security, ecological and environmental degradation, and economic losses (Adnan et al., 2018). Drought is defined broadly as precipitation that is less than usual or average in any place in the world for an extended period (Sirdas and Sen, 2003). The literature classifies drought as meteorological, hydrological, and agricultural. In addition, the socio-economic drought type that these three will affect is mentioned in the classifications. Meteorological drought is less precipitation than average in a region, hydrological drought is the deficiency of surface and underground water required for water supply, and agricultural drought is the inability of plants to find the water they need and, accordingly, the restriction of agricultural production. Socio-economic drought, conversely, refers to the negativities that occur

in social and economic life depending on other types of droughts (Arslan et al., 2016). Drought is one of the most tangible results of global climate change; it is imperative to identify and categorize temporal and spatial analysis, follow-up and observation, and creation of various projections with predictions for the future. Drought prediction and monitoring may be critical in managing water and land resources, significantly reducing damage (Fadaei-Kermani and Ghaeini-Hessaroeyeh, 2020). Information such as the impact area, severity, duration, and frequency of the drought can be obtained with the help of drought indexes used as a drought monitoring tool (Dogan et al., 2012). The Palmer drought severity index (PDSI) (Palmer, 1965), Erinç aridity index (EAII) (Erinc, 1995), standardized precipitation index (SPI) (McKee et al., 1993), China-Z index (CZI) (Ju et al., 1997), reconnaissance drought index (RDI) (Tsakiris and Vangelis, 2005), standardized streamflow index (SSI) (Shukla and Wood, 2008), streamflow drought index (SDI) (Nalbantis and Tsakiris, 2009), and the standardized precipitation evapotranspiration index (SPEI) (Vicente-Serrano et al., 2010) drought indexes are the most used

* Corresponding author.

E-mail address: hcitakoglu@erciyes.edu.tr (H. Citakoglu).

indexes in the literature.

While classical mathematical equations based on deterministic or stochastic models were used in the early periods of drought prediction studies, artificial intelligence methods have become extremely popular due to the developing technologies in the last thirty-year period. Artificial neural networks, genetic programming, fuzzy logic, expert systems, Gaussian processes, support vector machines, and the KNN algorithm are examples of machine learning (ML) approaches. These are used extensively in the hydrometeorological time series analysis in which artificial intelligence is considered. ML techniques have taken the place of linear approaches because they give more successful results than models such as the autoregressive integrated moving average (ARIMA) and autoregressive moving average (ARMA) in the prediction studies of nonlinear and nonstationary hydrometeorological data (Fung et al., 2020; Latifoğlu, 2022a; 2022b; 2022c). Because of their capacity to learn from observable data, ML techniques can also represent the intricate interconnections inherent in natural occurrences (Fung et al., 2020). Over the last two decades, ML techniques, particularly neural networks, have shown considerable promise in modeling nonlinear time series. However, when two or more hidden layers are necessary for very complicated phenomena, the issue of nonconvex optimization arises (Agana and Homaifar, 2017). Besides, deep learning (DL) algorithms, a subcategory of ML, when compared to simple neural network models, can automatically learn complicated temporal patterns through high-level abstraction and nonlinear modification and obtain approximations of complex functions (Li et al., 2020). DL algorithm is artificial learning obtained with multi-layer models, and it is an increased and improved version of the hidden layer in artificial neural networks (LeCun et al., 2015). Because of their high performance, deep neural networks (DNNs), convolution neural networks (CNNs), recurrent neural networks (RNNs), long short-term memory (LSTM), restricted Boltzmann machines (RBMs), auto-encoders (AE), and deep belief networks (DBNs) have been widely used in prediction studies over the last decade. Deep learning was first proposed in the 1980s; it has only recently gained popularity due to the large quantity of data and computing power necessary for training (Bashar, 2019). RNNs in these algorithms are well suited for sequences or time series data. RNNs are also known as neural networks with memory because they can learn long-term dependencies along sequences (Burkov, 1997). However, they have disadvantages, such as the vanishing gradient issue and memory constraints (Latifoğlu, 2022a; 2022b). LSTM is a superior evolution of RNNs that tackles RNN flaws by increasing the number of contacts per cell (Sattari et al., 2021). LSTM has the architectures of RNNs and has been developed to eliminate the disadvantages of RNNs. When there are unknown time lags and bounds between critical occurrences, the LSTM algorithm is ideally suited to learn from experience to categorize processes and anticipate time series (Hochreiter and Schmidhuber, 1997). Due to these features, LSTM has been a prevalent method in prediction studies for the last four-five years.

Poornima and Pushpalatha (2019) predicted the SPI and SPEI drought indexes using various parameters for 1958–2014 in the Hyderabad Region of India. They used multivariate input to compare the univariate ARIMA statistical model with the LSTM recurrent neural network model. This research concluded that the LSTM model gave better results on a longer time scale, i.e., 6 and 12 months, than the ARIMA model (Poornima and Pushpalatha, 2019). Abhirup et al. (2020) proposed stacked long short-term memory (S-LSTM) to predict SPI drought values in the New South Wales area of Australia, where severe droughts are experienced. Training data from 1901 to 2000 and test data from 2001 to 2018 were used in the model as input data. The findings were compared to prominent ML techniques like random forest (RF) and ANN to understand the capabilities of the S-LSTM approach. The analyses demonstrate that deep learning models outperform the other models and gain a superior knowledge of drought features, particularly at long periods when the S-LSTM model is utilized (Abhirup et al., 2020). Mokhtar et al. (2021) studied a combination of machine learning for

SPEI drought analysis in the Tibetan Plateau of China from 1980 to 2019. This study used four ML techniques of CNN, LSTM, RF, and the extreme gradient boost (XGB) to predict three and six-month droughts. Seven alternative scenarios with varying combinations depending on changeable meteorological circumstances were used as inputs to the prediction models. Among these scenarios, in scenario four, LSTM gave better results for SPEI-6 predictions (Mokhtar et al., 2021). Wu et al. (2021) conducted precipitation and drought studies based on monthly and yearly precipitation time series between 1967 and 2017 in three meteorological sites representing three climate types in northeastern China. China-Z Index (CZI) was used as the drought index. Wavelet transformation (WT), ARIMA, and LSTM techniques described the drought time series. A novel hybrid model, WT-ARIMA-LSTM (W-AL) of monthly precipitation time series, was constructed. Based on multiple climatic types and training/test set ratios, the suggested W-AL model outperformed the ARIMA and LSTM for monthly precipitation data prediction accuracy (Wu et al., 2021). Docheshmeh et al. (2022) researched the drought prediction ability of LSTM using monthly precipitation data from four Iranian sites. A prediction model based on LSTM, it is based on predicting droughts on the SPI-3, SPI-6, SPI-9, and SPI-12-month time scales. The proposed LSTM model was compared with the multivariate adaptive regression curve (MARS), extra tree (ET), and vector autoregressive approach (VAR) techniques considering numerical criteria. According to the findings, the LSTM method outperformed other techniques in predicting drought across all time scales (Docheshmeh et al., 2022). Danandeh et al. (2022) proposed a new intelligent deep learning model to predict three and six-month short-term meteorological drought at two research sites in Ankara, Türkiye. This deep learning model consists of a new hybrid intelligent model called convolutional long short-term memory (CNN-LSTM). The accuracy of the proposed model has been compared with methods such as artificial neural networks and genetic programming. The results showed that the CNN-LSTM outperformed all the benchmarks (Danandeh et al., 2022).

In this research, the short-term meteorological drought of Sakarya, Türkiye, was predicted using LSTM, one of the deep learning algorithms. SPI-1, SPI-3, and SPI-6-month time scales drought values on 1, 3, and 6-month time scales derived from the monthly precipitation data of the station between 1960 and 2020 were taken as input data, including training and test data in the LSTM model. This study aims to predict the short-term SPI drought values in a region for the first time in Türkiye using a standalone LSTM method. A comparison was made with the EMD-ELM hybrid model to show the success and prediction capacity of the standalone LSTM method in time series modeling. In addition, for the standalone LSTM prediction model discussed in this research, it was investigated whether the drought time series needed to be subjected to pre-processing techniques. Another aim of this study is to reveal the superiority of the LSTM method over other machine learning methods in drought prediction in drought studies.

2. Materials and methods

2.1. Study area, data collection, and evaluation

Sakarya, an important industrial city, was chosen as the study area. The data were based on monthly precipitation data from the Sakarya Meteorology Station between 1960 and 2020. The station is located at latitude 40°76' and longitude 30°39'; its geographic location is shown in Fig. 1. The altitude of the station is about 31 m.

The typical Black Sea climate, hot in summer and warm in winter, is seen in most of the province of Sakarya. In general, precipitation in the form of rain is observed in all seasons in the city, and dry periods are not observed. According to the observations of the State Meteorological Service (MGM) station from 1951 to 2021, the monthly average precipitation is 70.4 mm, and the annual total precipitation average is 840 mm. Considering that Türkiye's average areal precipitation value for

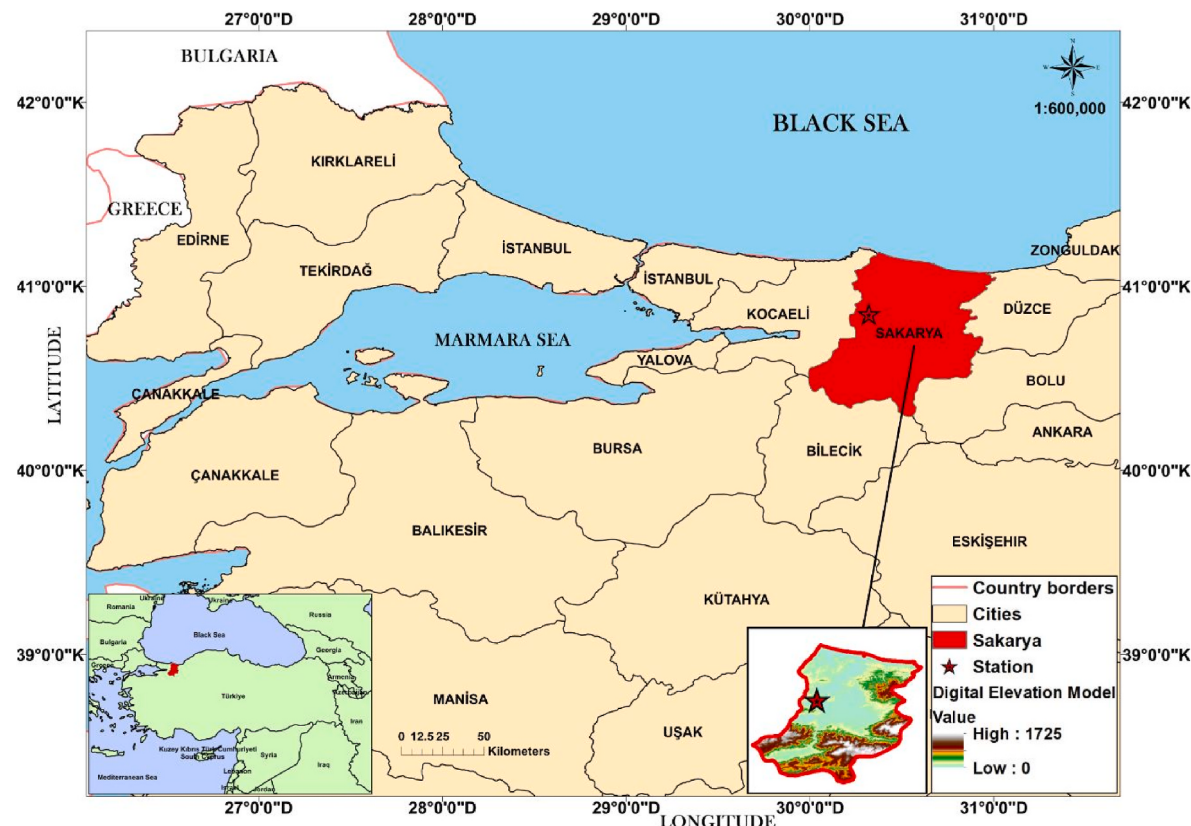


Fig. 1. Study area.

many years is 574 mm, the Sakarya province is well above Türkiye's average in terms of precipitation. The highest precipitation in one day was 127.7 mm on June 26, 1999. One hundred thirty days of the year are rainy throughout the province (Republic of Turkey, Ministry of Agriculture and Forestry General Directorate of Meteorology, 2022). The data set for the precipitation of the Sakarya Meteorology Station in the period 1960–2020 discussed in the study, was taken from the MGM. The annual total precipitation observed in Sakarya Meteorology Station from 1960 to 2020 is given in Fig. 2. As shown in Fig. 2, precipitation was well above the average in 1972, 1997, 2015, and 2016 and far below the average in 1966, 1985, 1993, 2006, 2011, and 2020.

There is no missing precipitation data in any month or year between 1960 and 2020, which was chosen as the observation period for Sakarya Meteorology Station. The Mockus equation (Zarei and Mahmoudi, 2021) was used to test the adequacy of the statistical period of the data set and was evaluated as appropriate. Sakarya's monthly precipitation in the Citakoglu and Coşkun (2022) study was also used as a dataset in this

study, and again the period of 1960–2020 is considered. In addition, before making prediction modeling with machine learning in their studies, Citakoglu and Coşkun (2022) performed Standard Normal Homogeneity, Mann–Whitney, Phillips–Perron, Augmented Dickey–Fuller, and Von Neumann's tests on the data. Citakoglu and Coşkun determined that this data set is homogeneous, stationary, and independent.

2.2. The standardized precipitation index (SPI)

McKee et al. (1993) created the SPI 1993 to define and observe drought. The World Meteorological Organization has emphasized this index as a starting point for observing meteorological drought. Because it depends only on monthly precipitation data, it is straightforward to compute and is widely accepted in precipitation drought analysis (Duvan et al., 2021; Elbeltagi et al., 2023; Lotfirad et al., 2022; Pande et al., 2023b). The SPI is a precipitation probability index that may be used for any time-period. The SPI is a probability index solely considering precipitation, whereas Palmer's indexes are water balance indexes that consider water supply precipitation, demand evapotranspiration, and loss (Zhai and Feng, 2009). Some arid regions are limited (Shaowei et al., 2013). SPI is a frequently used SPEI index, which is remarkably similar to SPI and is widely used in drought studies. While SPI only determines meteorological drought depending on precipitation, SPEI emphasizes the potential evapotranspiration (PET) parameter. Therefore, the SPEI's calculation is more complex. In addition, the applicability of SPEI in studies on meteorological drought is in the literature. The reasons why SPI is used so frequently are: it depends only on precipitation data, it can characterize meteorological drought in different climatic conditions, it provides early drought warning for different time scales, it is suitable for normal distribution, and it is easy to calculate (Sirdas, 2002). The SPI is calculated by subtracting the mean from the precipitation for the selected period and dividing the result by the standard deviation. With this method, the effect of the lack of

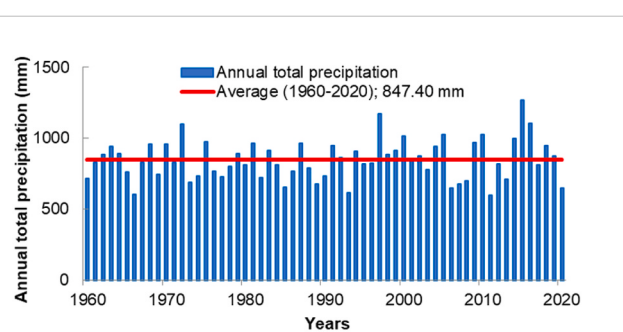


Fig. 2. Annual total precipitation in Sakarya Meteorology Station from 1960 to 2020.

precipitation on different sectors can be seen by examining different periods from 1 month to 48 months. Positive SPI numbers indicate more precipitation than the median, while negative values indicate less precipitation than the median. Wetter and drier climates can be depicted similarly since the SPI is standardized over a standard distribution (Poornima and Pushpalatha, 2019). The general categorization of SPI proposed (Adib and Marashi, 2019; Akturk et al., 2022; McKee et al., 1993; Zeybekoglu and Aktürk, 2021) is given in Table 1.

The first stage in calculating SPI is to choose a likelihood distribution that best matches the long-term time series of precipitation. The gamma distribution is recognized to fit the precipitation distribution accurately. For parameter fitting, maximum likelihood predictors are utilized.

The gamma function's likelihood density function is:

$$g(x) = \frac{1}{\beta^\alpha \Gamma(\alpha)} x^{\alpha-1} e^{-x/\beta} \text{ for } x > 0 \quad (1)$$

where α is a form parameter, β is a scale parameter, and x is the precipitation quantity. $\Gamma(\alpha)$ represents the gamma function, it is defined as:

$$\Gamma(\alpha) = \int_0^\infty y^{\alpha-1} e^{-y} dy \quad (2)$$

The distribution of the data must be anticipated. Edwards et al. (1997) propose predicting these parameters using an approximation for maximum likelihood (Edwards et al., 1997). Predictions of and generate a formula for the total probability $G(x)$ of an observed amount of precipitation for a particular month and time scale from the below mathematical activity.

$$G(x) = \int_0^x g(x) dx = \frac{1}{\beta^\alpha \Gamma(\alpha)} \int_0^x t^{\alpha-1} e^{-t/\beta} dt \quad (3)$$

$$G(x) = \frac{1}{\Gamma(\alpha)} \int_0^x t^{\alpha-1} e^{-t} dt \quad (4)$$

This is the incomplete gamma function. This value is determined using an algorithm adapted from (Press, 2007). Because the gamma distribution is undetermined for $x = 0$, and $q = P(x=0) > 0$ where $P(x=0)$ is the likelihood of no precipitation. Finally, the total likelihood distribution ($H(x)$) is calculated as follows.

$$H(x) = q + (1 - q) \cdot G(x) \quad (5)$$

In this equation, q represents the probability of a value of zero.

The SPI is then calculated by transforming the total likelihood distribution into the standard normal distribution. Considering the previously listed components, Lloyd-Hughes and Saunders provided the SPI calculation equation below (Lloyd-Hughes and Saunders, 2002; Pande et al., 2022):

$$SPI(t) = - \left(t - \frac{c_0 + c_1 \cdot t + c_2 \cdot t^2}{1 + d_1 + d_2 \cdot t^2 + d_3 \cdot t^3} \right) \text{ for } 0 < H(x) \leq 0.5 \quad (6)$$

Table 1
The SPI drought categorization (Ghasemi et al., 2022; Zarei, 2019).

SPI values	Drought category
>2	Extremely wet
1.5–1.99	Very wet
1–1.49	Moderately wet
-0.99–0.99	Near normal
-1 to -1.49	Moderately dry
-1.5 to -1.99	Severely dry
< -2	Extremely dry

$$SPI(t) = + \left(t - \frac{c_0 + c_1 \cdot t + c_2 \cdot t^2}{1 + d_1 + d_2 \cdot t^2 + d_3 \cdot t^3} \right) \text{ for } 0.5 < H(x) \leq 1 \quad (7)$$

where $c_0 = 2.51557$, $c_1 = 0.802853$, $c_2 = 0.010328$, $d_1 = 1.432788$, $d_2 = 0.189269$ and $d_3 = 0.001308$. The SPI(t) value shows the Z-score and is the positive or negative equivalent of the drought values. Also, t representing the time is derived from the following equations (McKee et al., 1993):

$$t = \sqrt{\ln \frac{1}{(H(x))^2}} \text{ for } 0 < H(x) \leq 0.5 \quad (8)$$

$$t = \sqrt{\ln \frac{1}{(1 - H(x))^2}} \text{ for } 0.5 < H(x) \leq 1 \quad (9)$$

3. Long short-term memory (LSTM)

The long-short-term memory (LSTM) is a deep learning algorithm introduced by Hochreiter and Schmidhuber in 1997. The model has been developed to solve the vanishing gradient and restricted memory capacity problems that traditional recurrent neural network (RNN) models encounter in predicting long-term time series. LSTM uses RNN architecture and is a special advanced type of RNN (Hochreiter and Schmidhuber, 1997). Deep features of LSTM architecture in time series may learn when to forget and how long to save the state information through the input, forget, and output gates and memory cells (Fan et al., 2020). The architecture of the LSTM model with one cell is shown in Fig. 3.

The mathematical explanation of the LSTM model with one-cell is briefly explained in the following order:

The LSTM architecture includes three gates that determine whether an input is important and decide whether to save it. The information is stored in one cell and sent to the next via gate controls. With the help of these gates, it is much simpler to examine information precisely. The x and $+$ symbols represent addition and multiplication operations in the model. The main notion of LSTM is Cell state (C_t), which carries information past the gates in an unaffected manner. The first gate is known as the forget gate, and it controls which units of the cell state vector C_{t-1} are forgotten. Equation (10) given below, explains the forgetting process (f_t):

$$f_t = \sigma(W_f \cdot [h_{t-1}, x_t] + b_f) \quad (10)$$

where f_t is the output vector, σ is the sigmoid function, W_f and b_f are the parameters for the first gate that can be taught. The value f_t , which runs from 0 to 1, indicates the degree of forgetting.

The input gate is the layer where added information is determined to be stored in the cell state. This layer takes in the data and learns new knowledge in addition to what it already knows from short-term mem-

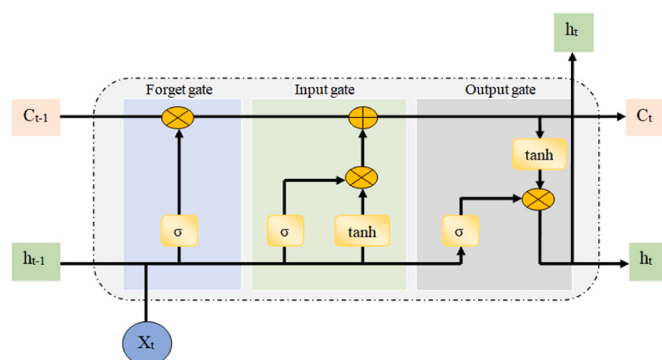


Fig. 3. The architecture of LSTM model with one-cell (Latifoglu, 2022a).

ory. The sigmoid layer called (i_t) is calculated as in equation (11).

$$i_t = \sigma \cdot (W_i \cdot [h_{t-1}, x_t] + b_i) \quad (11)$$

where i_t is a variable with a value between 0 and 1 as an output. W_i and b_i are the trainable variables. The current input x_t and the latest hidden state h_{t-1} are then used to generate a prospective vector of the cell state.

The tangent layer of the input gate is the layer where new candidate values (\tilde{C}) are created and are expressed as in equation (12).

$$\tilde{C} = \tanh \cdot (W_c \cdot [h_{t-1}, x_t] + b_c) \quad (12)$$

where \tilde{C} is a vector with 0–1 value, \tanh is the hyperbolic tangent and W_c and b_c are the trainable variables.

In the next step, the cell state vector entering the cell as C_{t-1} transforms into C_t based on data from other layers. The long-term memory is revamped in this step by adding the latest information to the sections from the long-term memory.

$$C_t = f \cdot C_{t-1} + i_t \cdot \tilde{C} \quad (13)$$

At the output gate, which is the last gate, the inputs (x_t and h_{t-1}) are transmitted through a sigmoid layer that determines how much the output of the output gate (O_t) is affected by the cell state. Finally, the cell state is transferred through the \tanh activation function and multiplied by the output value of the output gate to get h_t .

$$O_t = \sigma \cdot (W_o \cdot [h_{t-1}, x_t] + b_o) \quad (14)$$

$$h_t = O_t \cdot \tanh(C_t) \quad (15)$$

where O_t is a vector from 0 to 1 values, W_o and b_o are the trainable variables determined for the output gate (Docheshmeh et al., 2022; Fan et al., 2020; Latifoglu, 2022a; 2022b; Olah, 2015; Sattari et al., 2021).

3.1. Extreme learning machine (ELM)

Huang et al. (2006) introduced the Extreme Learning Machine (ELM) as a novel machine learning approach. The ELM is a single hidden layer ANN model faster than feed-forward back-propagation techniques and has more outstanding generalization capabilities. ELM's quick learning is because the mapping parameters between its input and hidden layers (hidden nodes) are determined at random at the start of the training (Huang et al., 2006). In other words, the concealed nodes are never modified and might be inherited unchanged from their predecessors (Gholizadeh et al., 2022). ELM has two basic training approaches, random initialization and linear parameter solutions. According to Huang et al. (2006), ELM is faster than classical neural networks because the learning of ELM has a one-pass algorithm without re-iteration. In this research, ELM was used to compare the prediction success of the LSTM model since it provides faster analysis, and the learning algorithms are more advanced than ANN. Further details about ELM can be found in (Demir and Citakoglu, 2022; Huang et al., 2006; Wang et al., 2022).

3.2. Empirical mode decomposition (EMD)

Empirical mode decomposition (EMD) is a data-adaptable pre-processing approach developed by (Huang et al., 1998). EMD decomposes a time series signal into different sub-signals: intrinsic mode functions (IMFs) and residuals with a shifting process. These decomposed sub-signals are similar in length and time scale to the original signal. Obtaining IMFs and residual signals with EMD consists of the following steps.

- i. The maximum and minimum extreme values of the original signal are determined.
- ii. These values are combined to obtain the lower and upper envelopes.

- iii. The average of the lower and upper envelopes is determined.
- iv. The average value calculated from the original signal is subtracted.
- v. The new value obtained is taken as the input signal, and this process continues until the average becomes zero.
- vi. Thus, the desired number of IMF signals is obtained.
- vii. The value remaining because of these operations is the residual signal.

The EMD technique is more favorable and effective than other pre-processing techniques because it can distinguish nonstationary and nonlinear signals. The EMD technique is more suited for evaluating nonstationary hydrological time series. The adaptive feature of the EMD technique based on data makes it superior to other techniques. The sifting process specific to the EMD approach eliminates oscillations passing through local maximums and minimums. It is also relatively fast at analyzing. Sometimes mode mixing issues can occur during the EMD process (Citakoglu and Coşkun, 2022; Lei et al., 2013; Yasir and Koh, 2018).

Detailed theoretical information about the EMD technique can be found in (Huang et al., 1998; Zhang et al., 2022).

3.3. Error criteria

The accuracy of the prediction models discussed in this research was evaluated with six different performance criteria commonly used in the literature. These are mean square error (MSE), root mean square error (RMSE), mean absolute error (MAE), Nash–Sutcliffe efficiency (NSE), the overall index of model performance (OI), and determination coefficient (R^2). Higher performances are achieved as MSE, RMSE, and MAE get closer to 0 and R² closer to 1. The NSE takes values between -∞ and 1. NSE values less than 0.5 are unsatisfactory performance, between 0.5 and 0.7 are acceptable, between 0.7 and 0.9 are high, and between 0.9 and 1 demonstrate exceptional performance (Nash and Sutcliffe, 1970; Özbayrak et al., 2023; Pande et al., 2023a). The OI takes values between -∞ and 1, and an OI value of 1 indicates excellent performance (Bayram et al., 2015; Citakoglu, 2015). The error criteria discussed in this study were calculated with the following equations:

$$MSE = \frac{1}{N} \sum_{N=1}^N (SPI_{pre} - SPI_{cal})^2 \quad (16)$$

$$RMSE = \sqrt{\frac{1}{N} \sum_{N=1}^N (SPI_{pre} - SPI_{cal})^2} \quad (17)$$

$$MAE = \frac{1}{N} \sum_{N=1}^N |SPI_{pre} - SPI_{cal}| \quad (18)$$

$$NSE = 1 - \frac{\sum_{N=1}^N (SPI_{pre} - SPI_{cal})^2}{\sum_{N=1}^N (SPI_{cal})^2} \quad (19)$$

$$OI = \frac{1}{2} \left(2 - \frac{RMSE}{(SPI_{cal,max} - SPI_{cal,min})} - \frac{\sum_{N=1}^N (SPI_{pre} - SPI_{cal})^2}{\sum_{N=1}^N (SPI_{cal})^2} \right) \quad (20)$$

$$R^2 = 1 - \frac{\sum_{N=1}^N (SPI_{pre} - SPI_{cal})^2}{\sum_{N=1}^N (SPI_{pre})^2} \quad (21)$$

The N shows the number of data sets used for the training and testing of models. SPI_{pre} is prediction values obtained from the models, SPI_{cal} is

drought values calculated from monthly precipitation data. \overline{SPI}_{pre} and \overline{SPI}_{cal} are the averages of predicted and calculated values. $SPI_{cal\ max}$ and $SPI_{cal\ min}$ are the minimum and maximum values of the calculated series.

4. Model development

This study is based on predicting the short-term meteorological drought of Sakarya, located in the northwest of Türkiye, using the LSTM model, which is one of the popular deep learning algorithms of the recent period. The flowchart of the study is given in Fig. 4.

In the current study, SPI-1, SPI-3, and SPI-6-month time scales (SPI for 1, 3, and 6 months) drought values calculated from monthly precipitation of Sakarya Meteorology Station recorded between 1960 and

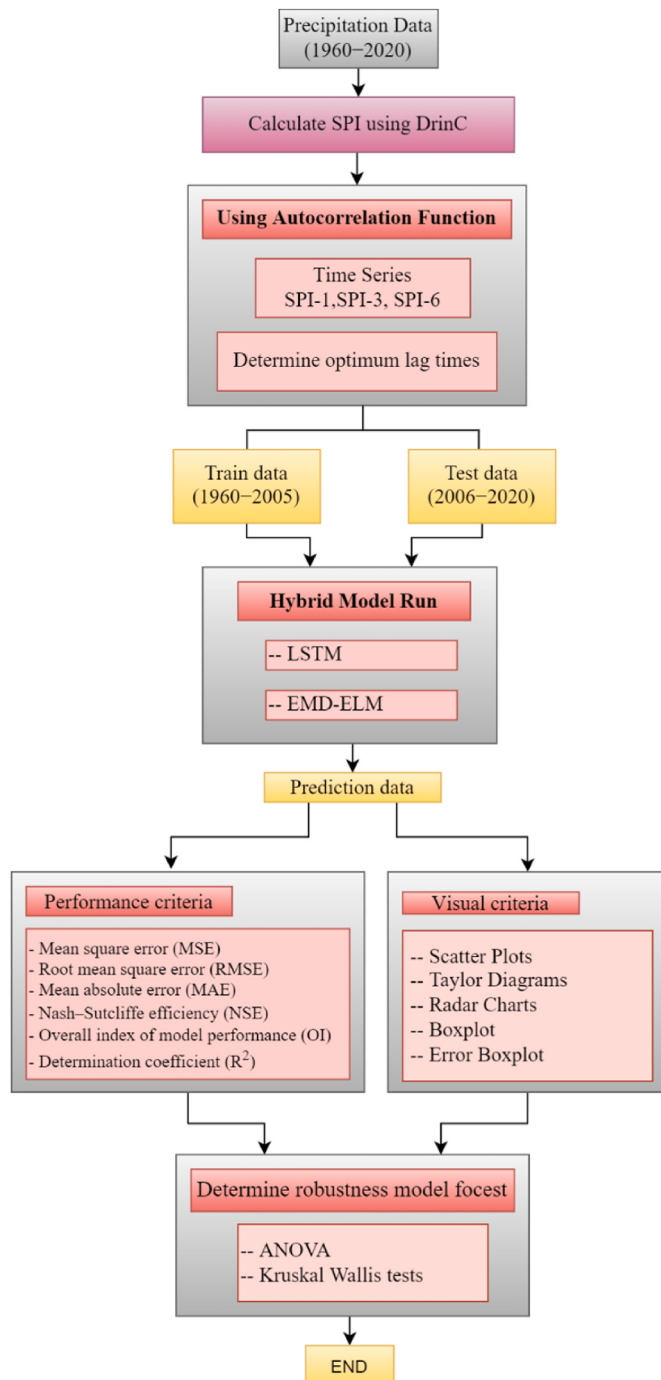


Fig. 4. Flowchart of study.

2020 were used. As seen in Fig. 4, the only parameter considered in the study's drought prediction is historical precipitations. SPI drought values were calculated practically with the Drought Indices Calculator (DrinC) software (Tigkas et al., 2015). DrinC software is accessible to all. DrinC software significantly reduced the processing and calculation time in calculating SPI values for SPI-1, SPI-3, and SPI-6-month time scales. After obtaining the SPI drought time series, the autocorrelation function (ACF) was used to determine the optimum lag times (input variables) (Başakın et al., 2022; Citakoglu, 2021; Demir, 2022; Demir and Yaseen, 2022). It is essential for the success of the prediction model how many prior months will be included in the input variables so that a future value can be predicted using historical data in time series. For this reason, optimum lag times (t , $t-1$, $t-2$, ..., $t-n$) were analyzed with the ACF to predict the drought value at $t+1$ lag time as the output variable. The codes of the graphics method in Matlab (2021b) software were used to determine the optimum lag times and to investigate the presence of autocorrelation between the time series.

SPI-1, SPI-3, and SPI-6-month time scales drought data were divided into two training data for 1960–2005 (75%) and test data for 2006–2020 (25%). The LSTM and EMD-ELM hybrid models used these datasets as input data. First, these training and test data were predicted with the LSTM model without normalization and pre-processing. The LSTM deep learning algorithm standardizes the data in itself. In the LSTM cell architecture proposed in the prediction study, the “sequence input layer” as the input layer, the “bidirectional LSTM (BiLSTM) layer” as the hidden layer, the “fully connected layer” as the connection layer, and the “regression layer” as output layer were used. The tanh and sigmoid functions were used for the cell’s state and gate activation functions. In the LSTM model, the maximum number of epochs was 200, the initial learning rate was 0.05, the learning rate drop period was 125, and the learning rate drop factor was 0.2. Predictions were obtained by trial and error with the number of neurons in the 5–25 with one hidden layer. In addition, three different learning algorithms were used to train the deep network in the LSTM model. Stochastic gradient descent with momentum (SGDM), root mean square propagation (RMSPROP), and adaptive moments (ADAM) learning algorithms were discussed, and the algorithm that gave the best result according to the error criteria was selected. The prediction process in the LSTM model was completed using the codes in the Matlab 2021b software.

To comprehend the prediction capacity of the LSTM model, the EMD-ELM hybrid model was used, and the results were compared. The first step in creating the hybrid model is the sub-bands of SPI-1, SPI-3, and SPI-6-month time scales drought data using the EMD pre-processing technique. The IMFs and residual components were obtained by dividing the drought time series into sub-bands from 2D, 3D, 4D, and 5D levels. IMFs and residual components at each level were used as input data in the ELM method, and predictions were obtained with this hybrid method. The normalization of the data was performed with the ELM method. Only a single hidden layer and a feed-forward learning network were used in the ELM method. In the ELM method, regression as the ELM type, 500 as the maximum number of neurons, and 0.70 as the learning rate were chosen.

The prediction success of the LSTM and the EMD-ELM hybrid models for each time scale was discussed according to error criteria, scatter plots, Taylor diagrams, and radar charts. The Taylor diagrams were used to evaluate the results obtained from the models with standard deviation and correlation. Scatter plots are used to show the calculated drought series and the predicted drought series together. Radar charts were used to show all error criteria together and comparatively.

5. Results and discussion

5.1. Results

Graphs of SPI-1, SPI-3, and SPI-6-month time scales calculated using DrinC software from monthly precipitation between 1960 and 2020 are

given in Fig. 5.

As can be seen from Fig. 5, the drought values calculated for the SPI-1, SPI-3, and SPI-6-month time scales are generally in the normal drought range. There is no apparent trend as a dry period or a wet period. While the peak values of drought are similar sometimes, they generally differ. The mean value for each time scale is 0, and the standard deviation is 1. Because SPI is a drought index suitable for normal distribution, DrinC software calculated SPI considering the normal

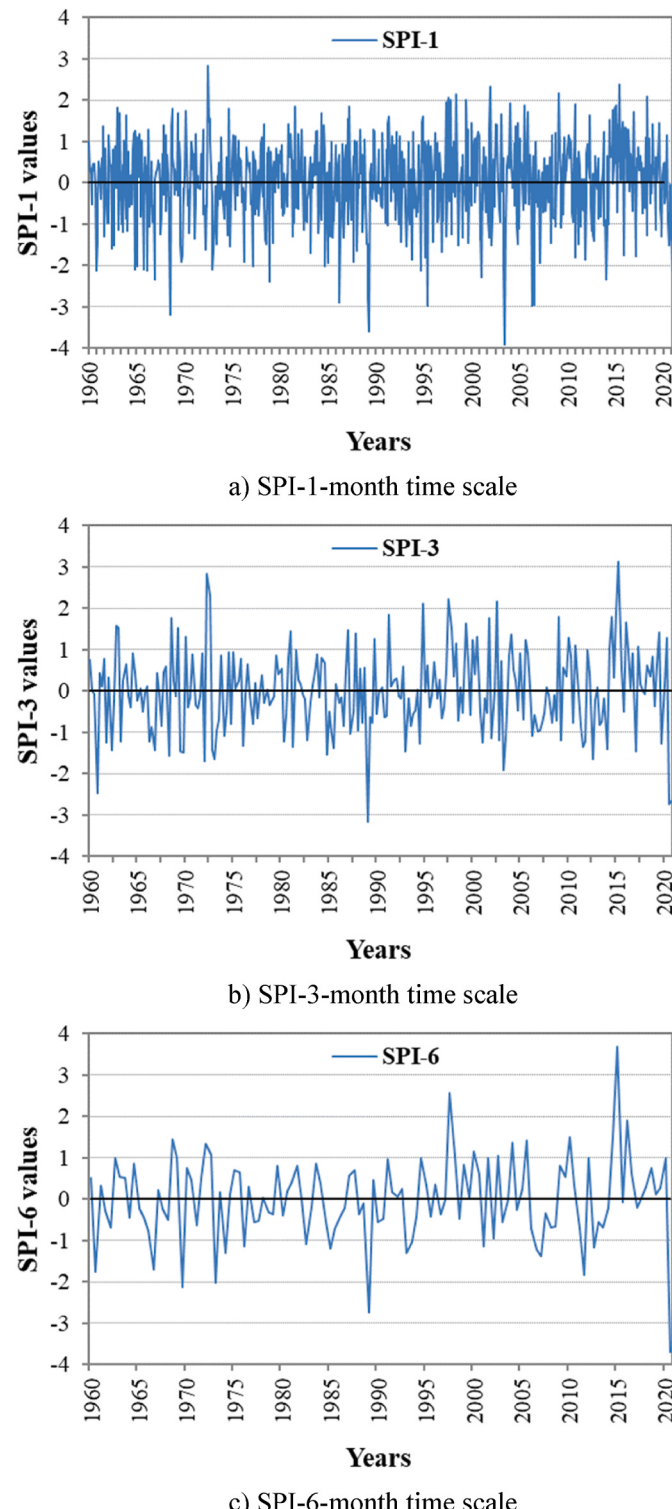


Fig. 5. Drought time series graphs a) SPI-1 b) SPI-3 c) SPI-6-month time scales.

distribution.

After calculating the drought time series, the autocorrelation function was applied to these series to determine the optimum lag times to be used as input data in the prediction models. Sample autocorrelation function graphs for each time scale are given in Fig. 6.

As shown in Fig. 6, autocorrelation was investigated up to the 20th lag time in the drought time series of SPI-1, SPI-3, and SPI-6-month time scales. All lag times up to the considered 20th lag time remained within the confidence interval. The original drought time series did not correlate with each other at various times. For this reason, all lag times up to the 20th lag time considered can be taken as input variables in the prediction models. According to the results obtained, optionally, t , $t-1$, $t-2$, and $t-3$ values were selected as input variables, and $t+1$ time was chosen as output variable.

First, the LSTM prediction model was run according to the input and output variables, and predictions were obtained for each time scale. The results of the predictions obtained according to the training and test data in the LSTM prediction model, according to the error criteria, are given

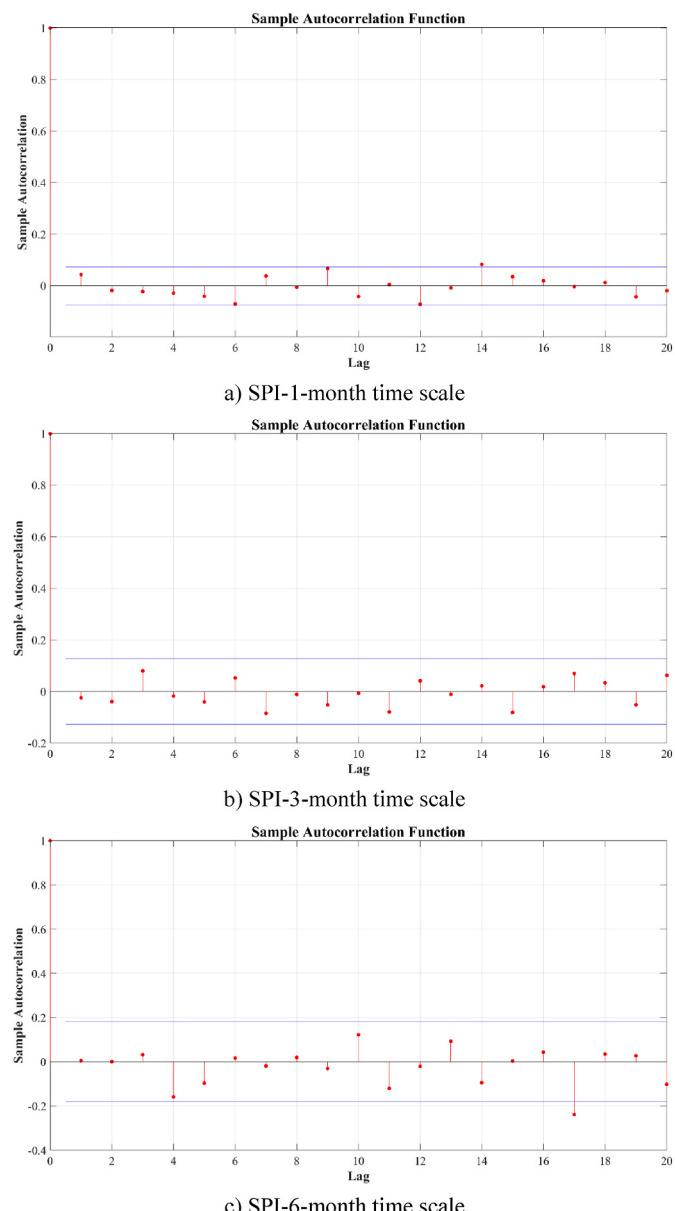


Fig. 6. Sample autocorrelation graphs of drought time series a) SPI-1 b) SPI-3 c) SPI-6-month time scales.

Table 2.

As shown in [Table 2](#), the training ability of the applied LSTM prediction model gave extraordinarily successful results for each time scale and each input variable. In addition, although the test performance of the model was lower than the training performance, it still gave remarkably successful results. According to the test results, three inputs ($t, t-1, t-2, t-3$ variables) in a 1-month time scale, two inputs ($t, t-1, t-2$ variables) in an SPI-3-month time scale, and one input ($t, t-1$ variables) in an SPI-6-month time scale gave the highest results. The MSE, RMSE, NSE, OI, MAE, and R^2 values of the three inputs that gave the best results on an SPI-1-month time scale were found to be 0.03, 0.17, 0.97, 0.97, 0.11, and 0.97. The MSE, RMSE, NSE, OI, MAE, and R^2 values of the two inputs that gave the best results on an SPI-3-month time scale were found to be 0.10, 0.32, 0.92, 0.93, 0.18, and 0.94. The MSE, RMSE, NSE, OI, MAE, and R^2 values of the one input that gave the best results on an SPI-6-month time scale were found to be 0.31, 0.56, and 0.81, respectively 0.87, 0.28 and 0.90.

Although the ELM method makes fast analyses thanks to its high generalization ability, it is not usually used alone in time series. Because the input weights and biases are chosen randomly, the output of ELM differs from time to time. For time series issues, it is frequently used in combination with pre-processing techniques like DWT, EMD, and VMD to boost ELM's generalization capabilities. When ELM is used with these pre-processing techniques, the performance criteria of prediction models are greatly improved. In addition to all these reasons, the EMD-ELM hybrid model was preferred in this research because the EML technique is understandable and easy to apply ([Li et al., 2018](#); [Lian et al., 2013](#); [Lu and Shao, 2012](#); [Sahani et al., 2020](#); [Seo et al., 2018](#); [Yang and Chen, 2019](#)).

The EMD-ELM hybrid model, another prediction model discussed in the research, was utilized to compare the prediction capability of the LSTM model. The error criteria for the prediction results on the SPI-1, SPI-3, and SPI-6-month scales obtained from this hybrid model are in [Tables 3–5](#).

As can be seen in [Table 3](#), according to the error criteria of the predictions obtained from the EMD-ELM hybrid model on the SPI-1-month time scale, the 5th band level of EMD at input times 1 and 2, and the 2nd band level of EMD at input time 3 gave the best results. As seen in [Table 4](#), the 4th band level of EMD at input time 1 and the 3rd band level of EMD at input times 2 and 3 gave the best results on the 3-

Table 3

Error criteria for SPI-1-month time scale of the applied EMD-ELM hybrid model.

Inputs	Output	EMD Band Levels	TRAINING					
			MSE	RMSE	NSE	OI	MAE	R^2
t, t-1	t+1	2D	0.13	0.35	0.87	0.91	0.28	0.91
		3D	0.13	0.36	0.87	0.91	0.29	0.91
		4D	0.13	0.36	0.87	0.91	0.29	0.91
		5D	0.05	0.23	0.94	0.96	0.19	0.96
t, t-1, t-2	t+1	2D	0.15	0.38	0.85	0.90	0.36	0.98
		3D	0.15	0.38	0.85	0.90	0.32	0.94
		4D	0.15	0.38	0.85	0.90	0.32	0.94
		5D	0.14	0.38	0.85	0.90	0.32	0.94
t, t-1, t-3	t+1	2D	0.15	0.38	0.85	0.90	0.36	0.98
		3D	0.13	0.36	0.87	0.91	0.28	0.93
		4D	0.13	0.36	0.87	0.91	0.28	0.93
		5D	0.13	0.36	0.87	0.91	0.28	0.93
TEST								
t, t-1	t+1	2D	0.35	0.60	0.63	0.76	0.49	0.89
		3D	0.27	0.52	0.71	0.81	0.41	0.86
		4D	0.24	0.49	0.75	0.83	0.38	0.87
		5D	0.09	0.29	0.91	0.93	0.24	0.94
t, t-1, t-2	t+1	2D	0.25	0.50	0.73	0.82	0.38	0.87
		3D	0.28	0.53	0.71	0.80	0.42	0.87
		4D	0.25	0.50	0.75	0.83	0.38	0.87
		5D	0.24	0.48	0.76	0.83	0.36	0.87
t, t-1, t-3	t+1	2D	0.22	0.41	0.90	0.90	0.30	0.92
		3D	0.25	0.50	0.84	0.82	0.32	0.90
		4D	0.23	0.48	0.76	0.83	0.39	0.90
		5D	0.22	0.47	0.77	0.84	0.37	0.90

month time scale. As seen in [Table 5](#), the 4th band level of EMD at input time 1, the 3rd band level of EMD at input time 2, and the 3rd band level of EMD at input time 3 gave the best results on the 6-month time scale.

The best results obtained in the EMD-ELM hybrid model according to different EMD band levels were compared with those in the LSTM prediction model. A comparison of the error criteria of the test results obtained from both the LSTM model and the EMD-ELM hybrid model is given in [Table 6](#).

As shown in [Table 6](#), the three input times ($t, t-1, t-2, t-3$) of the LSTM

Table 2

Error criteria for each time scale of the applied LSTM prediction model.

Month Time Scales	Inputs	Output	TRAINING					
			MSE	RMSE	NSE	OI	MAE	R^2
SPI-1	t, t-1	t+1	0.01	0.08	0.99	0.99	0.05	0.99
	t, t-1, t-2	t+1	0.01	0.07	0.99	0.99	0.04	1.00
	t, t-1, t-2, t-3	t+1	0.03	0.17	0.97	0.97	0.12	0.97
SPI-3	t, t-1	t+1	0.02	0.13	0.98	0.98	0.11	0.99
	t, t-1, t-2	t+1	0.01	0.07	0.99	0.99	0.05	0.99
	t, t-1, t-2, t-3	t+1	0.016	0.12	0.98	0.98	0.11	0.99
SPI-6	t, t-1	t+1	0.01	0.11	0.98	0.98	0.10	1.00
	t, t-1, t-2	t+1	0.01	0.041	1.00	0.99	0.03	1.00
	t, t-1, t-2, t-3	t+1	0.01	0.051	1.00	0.99	0.05	1.00
Month Time Scales								
SPI-1	—	—	MSE	RMSE	NSE	OI	MAE	R^2
	t, t-1	t+1	0.04	0.20	0.96	0.96	0.12	0.97
	t, t-1, t-2	t+1	0.04	0.20	0.96	0.96	0.11	0.96
SPI-3	t, t-1, t-2, t-3	t+1	0.03	0.17	0.97	0.97	0.11	0.97
	t, t-1	t+1	0.19	0.44	0.84	0.88	0.28	0.88
	t, t-1, t-2	t+1	0.10	0.32	0.92	0.93	0.18	0.94
SPI-6	t, t-1, t-2, t-3	t+1	0.20	0.44	0.84	0.88	0.19	0.86
	t, t-1	t+1	0.31	0.56	0.81	0.87	0.28	0.90
	t, t-1, t-2	t+1	0.47	0.68	0.72	0.82	0.40	0.84
	t, t-1, t-2, t-3	t+1	0.34	0.59	0.79	0.86	0.38	0.85

Table 4

Error criteria for SPI-3-month time scale of the applied EMD-ELM hybrid model.

Inputs	Output	EMD Band Levels	TRAINING					
			MSE	RMSE	NSE	OI	MAE	R ²
t, t-1	t+1	2D	0.12	0.35	0.87	0.90	0.29	0.91
		3D	0.14	0.38	0.84	0.89	0.30	0.90
		4D	0.15	0.39	0.84	0.89	0.31	0.90
		5D	0.15	0.39	0.84	0.88	0.31	0.90
t, t-1, t-2	t+1	2D	0.12	0.35	0.87	0.90	0.28	0.91
		3D	0.31	0.56	0.67	0.79	0.50	0.94
		4D	0.31	0.56	0.66	0.78	0.50	0.94
		5D	0.32	0.56	0.66	0.78	0.50	0.94
t, t-1, t-2, t-3	t+1	2D	0.36	0.60	0.62	0.76	0.59	0.97
		3D	0.11	0.33	0.88	0.91	0.26	0.94
		4D	0.08	0.28	0.92	0.93	0.21	0.95
		5D	0.08	0.28	0.92	0.93	0.21	0.95
TEST								
t, t-1	t+1	2D	0.20	0.45	0.80	0.84	0.38	0.92
		3D	0.17	0.41	0.83	0.87	0.35	0.94
		4D	0.16	0.40	0.84	0.88	0.34	0.95
		5D	0.19	0.43	0.81	0.86	0.37	0.93
t, t-1, t-2	t+1	2D	0.30	0.55	0.75	0.83	0.54	0.97
		3D	0.30	0.54	0.76	0.83	0.49	0.90
		4D	0.64	0.80	0.48	0.67	0.79	0.89
		5D	0.61	0.78	0.51	0.69	0.76	0.87
t, t-1, t-2, t-3	t+1	2D	0.38	0.62	0.66	0.78	0.61	0.98
		3D	0.25	0.50	0.77	0.84	0.46	0.93
		4D	0.89	0.94	0.20	0.52	0.91	0.90
		5D	0.74	0.86	0.34	0.60	0.83	0.95

Table 5

Error criteria for SPI-6-month time scale of the applied EMD-ELM hybrid model.

Inputs	Output	EMD Band Levels	TRAINING					
			MSE	RMSE	NSE	OI	MAE	R ²
t, t-1	t+1	2D	0.09	0.31	0.88	0.91	0.25	0.92
		3D	0.10	0.32	0.87	0.90	0.26	0.92
		4D	0.11	0.33	0.86	0.90	0.26	0.92
		5D	0.14	0.38	0.81	0.87	0.29	0.87
t, t-1, t-2	t+1	2D	0.61	0.78	0.18	0.51	0.78	0.97
		3D	0.21	0.46	0.72	0.82	0.42	0.93
		4D	0.20	0.44	0.74	0.83	0.40	0.93
		5D	0.29	0.54	0.60	0.75	0.47	0.85
t, t-1, t-2, t-3	t+1	2D	0.25	0.50	0.67	0.79	0.50	0.97
		3D	0.21	0.46	0.72	0.82	0.44	0.97
		4D	0.10	0.32	0.87	0.90	0.29	0.95
		5D	0.20	0.44	0.74	0.83	0.37	0.88
TEST								
t, t-1	t+1	2D	0.14	0.37	0.89	0.91	0.34	0.94
		3D	0.11	0.33	0.91	0.92	0.27	0.94
		4D	0.06	0.25	0.95	0.95	0.22	0.96
		5D	0.22	0.47	0.82	0.87	0.42	0.89
t, t-1, t-2	t+1	2D	0.65	0.81	0.61	0.75	0.71	0.88
		3D	0.18	0.43	0.89	0.92	0.32	0.90
		4D	0.47	0.69	0.72	0.81	0.64	0.89
		5D	0.84	0.91	0.50	0.69	0.88	0.85
t, t-1, t-2, t-3	t+1	2D	0.26	0.51	0.85	0.89	0.49	0.95
		3D	0.08	0.28	0.95	0.96	0.22	0.95
		4D	0.09	0.30	0.95	0.95	0.20	0.96
		5D	0.18	0.42	0.89	0.92	0.35	0.91

model gave the best results on the SPI-1-month time scale according to the error criteria. The MSE, RMSE, NSE, OI, MAE, and R² values of the three inputs that gave the best results on an SPI-1-month time scale were

found to be 0.03, 0.17, 0.97, 0.97, 0.11, and 0.97. The two input times (t, t-1, t-2) of the LSTM model gave the best results on the SPI-3-month time scale. The MSE, RMSE, NSE, OI, MAE, and R² values of the two inputs that gave the best results on an SPI-3-month time scale were found to be 0.10, 0.32, 0.92, 0.93, 0.18, and 0.94. And finally, the one input time (t, t-1) of the EMD-ELM hybrid model gave the best results on the 6-month time scale. The MSE, RMSE, NSE, OI, MAE, and R² values of the one input that gave the best results on a 6-month time scale were found to be 0.06, 0.25, 0.95, 0.95, 0.22, and 0.96. Another result obtained from Table 6 is that the prediction performance of the LSTM model decreased as the time scale increased, while the prediction performance of the EMD-ELM hybrid model increased.

Scatter and time series plots of the best test results obtained from the models on each time scale are given in Figs. 7–9.

As can be seen in Fig. 7, the regression line between the prediction values obtained in the LSTM model and the calculated values strongly intersects the linear curve ($y = x$ (45°)) on the 1-month time scale. In addition, as can be seen from the time series plots, the prediction values obtained in the LSTM model show a little deviation from the calculated values. In the EMD-ELM hybrid model, the regression line between the predicted and calculated values does not precisely intersect with the linear curve. As can be seen in Fig. 8, the regression line between the prediction values obtained in the LSTM model and the calculated values overlaps the linear curve more strongly than that of the EMD-ELM hybrid model on the 3-month time scale. Although the R² value of the EMD-ELM hybrid model is greater than the LSTM model's, the deviation is less in the LSTM model than in the EMD-ELM hybrid model according to the time series plots. As seen in Fig. 9, in contrast to the SPI-1 and SPI-3-month time scales, the prediction results obtained in the EMD-ELM hybrid model on the SPI-6-month time scale are superior to the prediction results obtained from the LSTM model. The regression line in the LSTM model could not precisely intersect with the linear curve on this time scale. The deviation in the linear curve and the time series is more significant than in the EMD-ELM hybrid model. Although the highest R² value is reached in this time scale among the scatter plots, the regression line and the linear curve do not strongly overlap in the EMD-ELM hybrid model. In addition, as seen in Fig. 8a and 9a, the LSTM model failed to predict the extreme values of the original SPI drought data.

Taylor diagrams are given in Fig. 10 to evaluate and compare the test results of the models. Calculated SPI drought values and prediction values obtained from LSTM and EMD-ELM hybrid models were analyzed in detail in these diagrams according to standard deviation, correlation coefficient, and centered root mean square difference (RMSD) statistical criteria.

As shown in Fig. 10a), the predicted results of the LSTM model gave results closer to the calculated values on the 1-month time scale. As shown in Fig. 10b), the R² values of the LSTM model and the EMD-ELM hybrid model are remarkably close to each other on the 3-month time scale. However, when examined together with other error criteria, it is seen that the LSTM model is superior to the EMD-ELM hybrid model. As can be seen in Fig. 10 c), the EMD-ELM hybrid model made far better predictions than the LSTM model on the 6-month time scale.

Radar charts are given in Fig. 11 to compare the error criteria of the best test results at SPI-1, SPI-3, and SPI-6-month time scales obtained from the LSTM model and the EMD-ELM hybrid model together. As shown in Fig. 11, considering all the error criteria, the LSTM model on the SPI-1 and SPI-3-month time scales and the EMD-ELM hybrid model on the SPI-6-month time scale showed superior prediction performances.

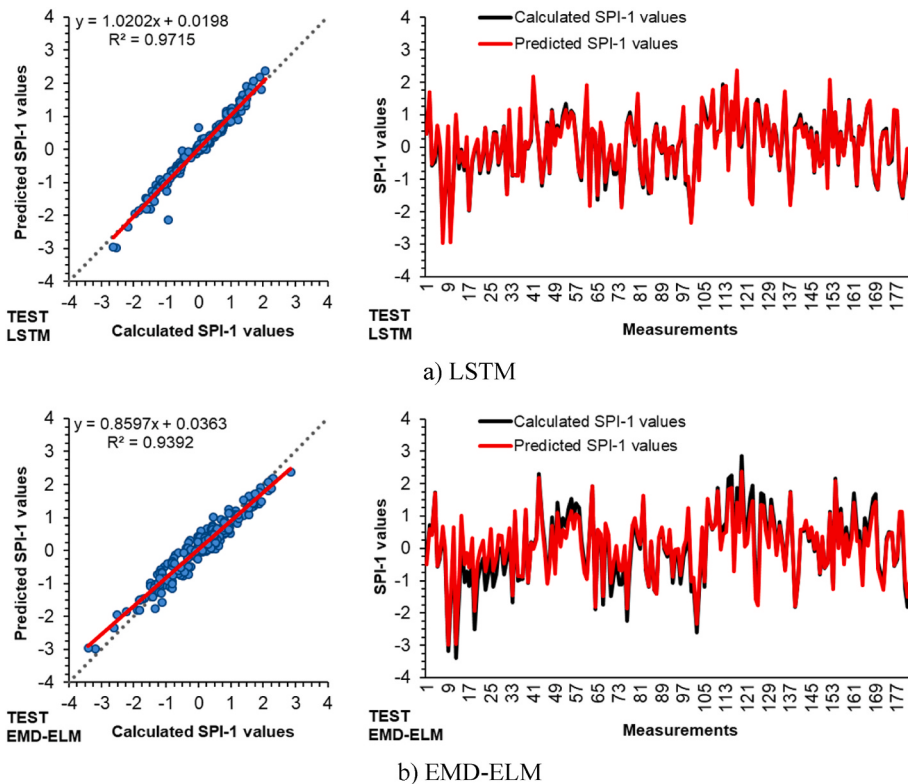
Fig. 12, 13, and 10 show the study's final results, including boxplot diagrams of standalone and hybrid models and error boxplot diagrams of these models. Model boxplot and error boxplot diagrams of LSTM models are identical on the three-time scales, as shown in Figs. 12–14. The boxplot diagram results coincide with the Taylor diagram results, as can be seen from these results.

One-way analysis of variance (ANOVA) and Kruskal-Wallis tests

Table 6

Comparison of the test performances of the LSTM model and EMD-ELM hybrid model.

Models	Month Time Scales	Inputs	Output	TEST					
				MSE	RMSE	NSE	OI	MAE	R ²
LSTM	SPI-1	t, t-1	t+1	0.04	0.20	0.96	0.96	0.12	0.97
		t, t-1, t-2	t+1	0.04	0.20	0.96	0.96	0.11	0.96
		t, t-1, t-2, t-3	t+1	0.03	0.17	0.97	0.97	0.11	0.97
	SPI-3	t, t-1	t+1	0.19	0.44	0.84	0.88	0.28	0.88
		t, t-1, t-2	t+1	0.10	0.32	0.92	0.93	0.18	0.94
		t, t-1, t-2, t-3	t+1	0.20	0.44	0.84	0.88	0.19	0.86
	SPI-6	t, t-1	t+1	0.31	0.56	0.81	0.87	0.28	0.90
		t, t-1, t-2	t+1	0.47	0.68	0.72	0.82	0.40	0.84
		t, t-1, t-2, t-3	t+1	0.34	0.59	0.80	0.86	0.38	0.85
EMD-ELM	SPI-1	t, t-1	t+1	0.08	0.29	0.91	0.93	0.24	0.94
		t, t-1, t-2	t+1	0.24	0.48	0.76	0.83	0.36	0.87
		t, t-1, t-2, t-3	t+1	0.22	0.41	0.90	0.90	0.30	0.92
	SPI-3	t, t-1	t+1	0.16	0.40	0.84	0.88	0.34	0.95
		t, t-1, t-2	t+1	0.30	0.54	0.76	0.83	0.49	0.90
		t, t-1, t-2, t-3	t+1	0.25	0.50	0.77	0.84	0.46	0.93
	SPI-6	t, t-1	t+1	0.06	0.25	0.95	0.95	0.22	0.96
		t, t-1, t-2	t+1	0.18	0.43	0.89	0.92	0.32	0.90
		t, t-1, t-2, t-3	t+1	0.08	0.28	0.95	0.96	0.22	0.95

**Fig. 7.** Scatter and time series plots of the best results on the SPI-1-month time scale a) LSTM b) EMD-ELM.

were used to examine the test results of the applied models to determine the significance of differences between the measured and estimated drought values of Machine Learning models (Bayram and Çitakoglu, 2023; Çitakoglu, 2021; Demir and Çitakoglu, 2022; Kisi et al., 2017). The test data are shown in Table 7 at a 95% significance level in the ANOVA test. According to the ANOVA, the LSTM model for the three-time scale drought accepts the H_0 hypothesis. In other words, the distribution of the means for the LSTM models and the three-time scale drought values are identical. The H_0 hypothesis is also accepted in the EMD-ELM model for 1 and 6-time scale drought; the H_0 hypothesis is rejected in the SPI-3-time scale drought. Then, the Kruskal-Wallis test

was used to determine if the estimated and measured data distributions were the same. As seen in Table 8, the H_0 hypothesis is rejected in the estimates of the drought data with LSTM and EMD-ELM models. In Table 8, the LSTM and EMD-ELM approach for all time scales passed the Kruskal-Wallis test except for the SPI-3-month time scale. According to the Kruskal-Wallis test results, the estimates given by these methods come from the same average as the measured drought values.

5.2. Discussion

The accuracy of the model results has not been investigated in

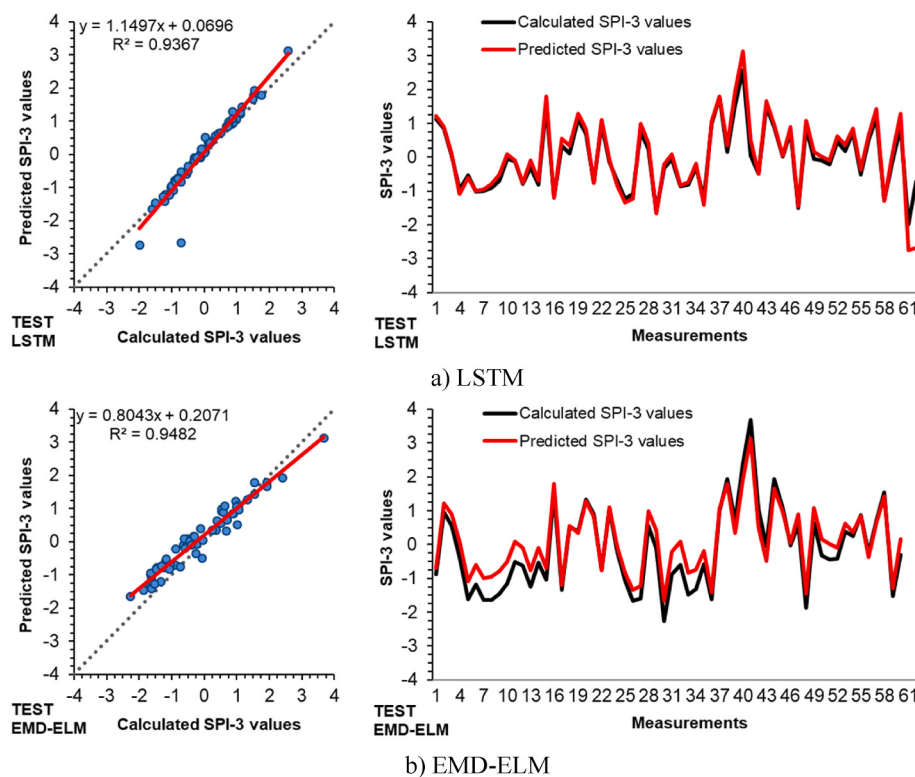


Fig. 8. Scatter and time series plots of the best results on the SPI-3-month time scale a) LSTM b) EMD-ELM.

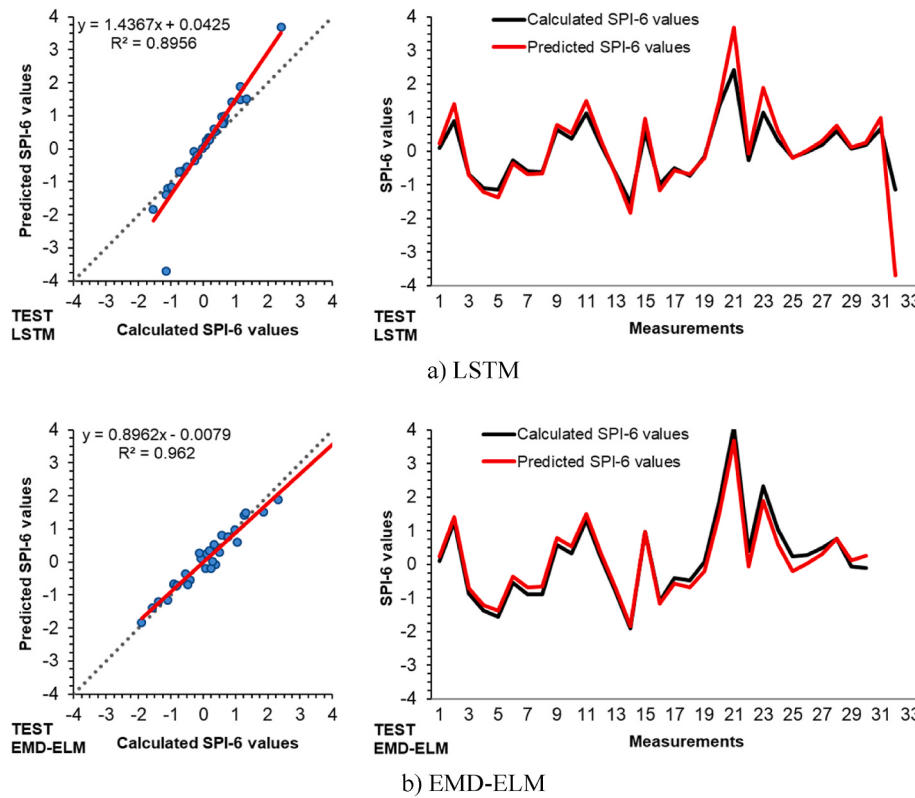


Fig. 9. Scatter and time series plots of the best results on the SPI-6-month time scale a) LSTM b) EMD-ELM.

drought prediction studies in the region (Danandeh et al., 2022; Ham et al., 2022; Özger et al., 2020; Poornima and Pushpalatha, 2019). In this study, the results of LSTM and EMD-ELM models were confirmed by

ANOVA and Kruskal-Wallis tests. With ANOVA and Kruskal-Wallis test, it was determined that the results of the LSTM model represent real data. Ham et al. (2022) stated that using the LSTM model to predict short-term

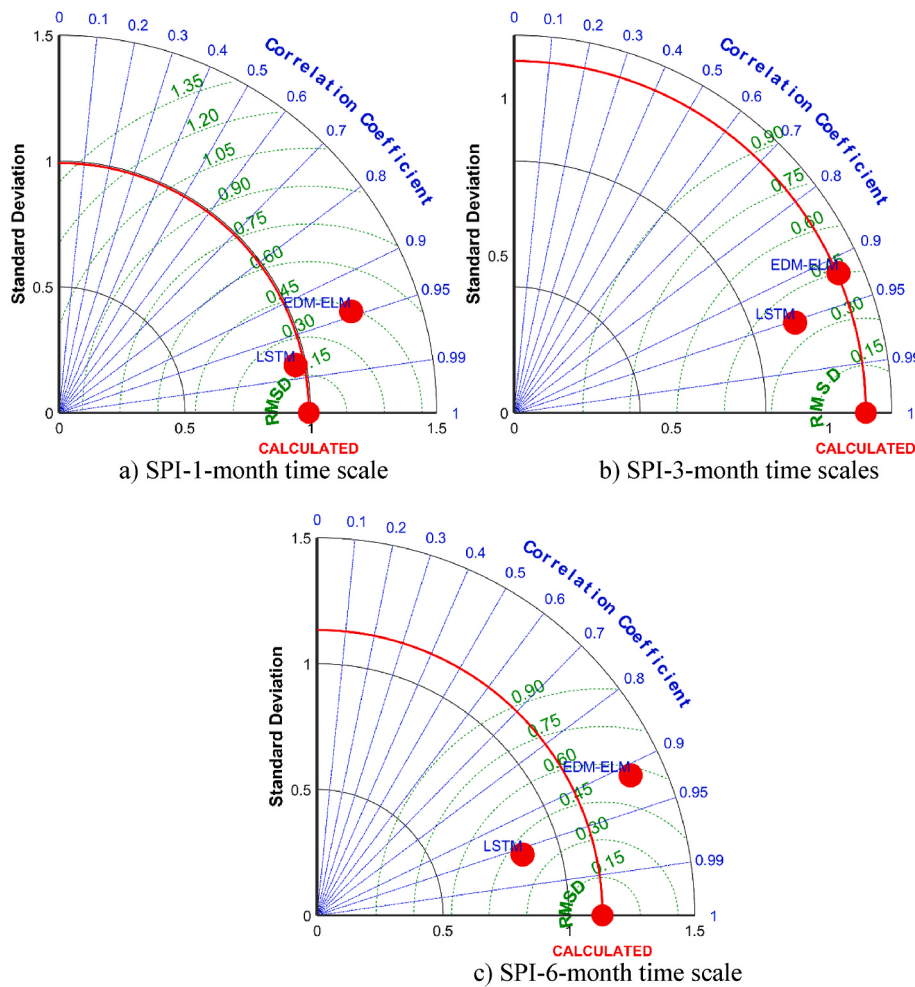


Fig. 10. Taylor diagrams of SPI test results on 1, 3 and 6-month time scales a) SPI-1 b) SPI-3 c) SPI-6-month time scales.

SPI values was more dependable.

Ham et al. (2022) stated that there was no significant improvement in the performance measures of LSTM due to the short data set. In this study, the standalone LSTM model's performance criteria are more satisfactory than the results of the EMD-ELM hybrid model. In time series predictions, the standalone LSTM model can overcome the deficiency of traditional machine learning models such as ANN, SVM, and ANFIS (Du et al., 2018; Ham et al., 2022; Zhao et al., 2019). By pre-processing the input data with EMD, ELM was comparable to LSTM in predicting the SPI time series.

Docheshmeh et al. (2022) predicted the drought series of SPI-3, SPI-6, SPI-9, and SPI-12-month time scales by LSTM, extra-trees (ET), vector autoregressive approach (VAR) and multivariate adaptive regression spline (MARS) methods. They stated that the LSTM method generally outperformed the other three methods.

Anshuka et al. (2019) stated that the smaller the temporal scale, the larger the prediction error. However, in this study, unlike that study, performance success decreases as the time scale increases. This result was also observed in other stations belonging to Türkiye (Danandeh et al., 2022; Özger et al., 2020). In addition, this result obtained with the LSTM method shows that the drought prediction performance for the SPI-1-month time scale is better than for SPI-3 and SPI-6-month time scales. Performance criteria of drought prediction study at the Sakarya station (Danandeh et al., 2022; Katipoğlu, 2023; Özger et al., 2020), in 2023 studies were determined to be more successful than other stations in Türkiye. This is because the studies are predictions of different drought indices.

6. Conclusion

In the present research, the short-term meteorological drought of Sakarya province was predicted for the SPI-1, SPI-3, and SPI-6-month time scales. In this drought prediction study, the LSTM method's prediction capability, one of the popular deep learning algorithms of the last period, has been investigated. The prediction ability of the LSTM model was compared with the EMD-ELM hybrid method. SPI-1, SPI-3, and SPI-6-month time scales drought data calculated from the monthly precipitation data of the Sakarya Meteorology Station between 1960 and 2020 were used as a variable in the prediction models. SPI-1, SPI-3, and SPI-6-month time scales drought data were divided into two as training data for 1960–2005 (75%) and test data for 2006–2020 (25%). Drought at $t+1$ output time was predicted using SPI values at t , $t-1$, $t-2$, and $t-3$ lag times as input variables. The prediction performances of the models were evaluated according to six different error criteria, Taylor diagrams, scatter plots, and radar charts. As a result of all these evaluations, the following conclusions were reached.

- The applied LSTM model is quite successful in terms of training ability.
- The LSTM model gave more successful results on the SPI-1 and SPI-3-month time scales.
- In the EMD-ELM hybrid model, when the results of four different (2D, 3D, 4D, 5D)

EMD band levels were examined for each time scale and each lag

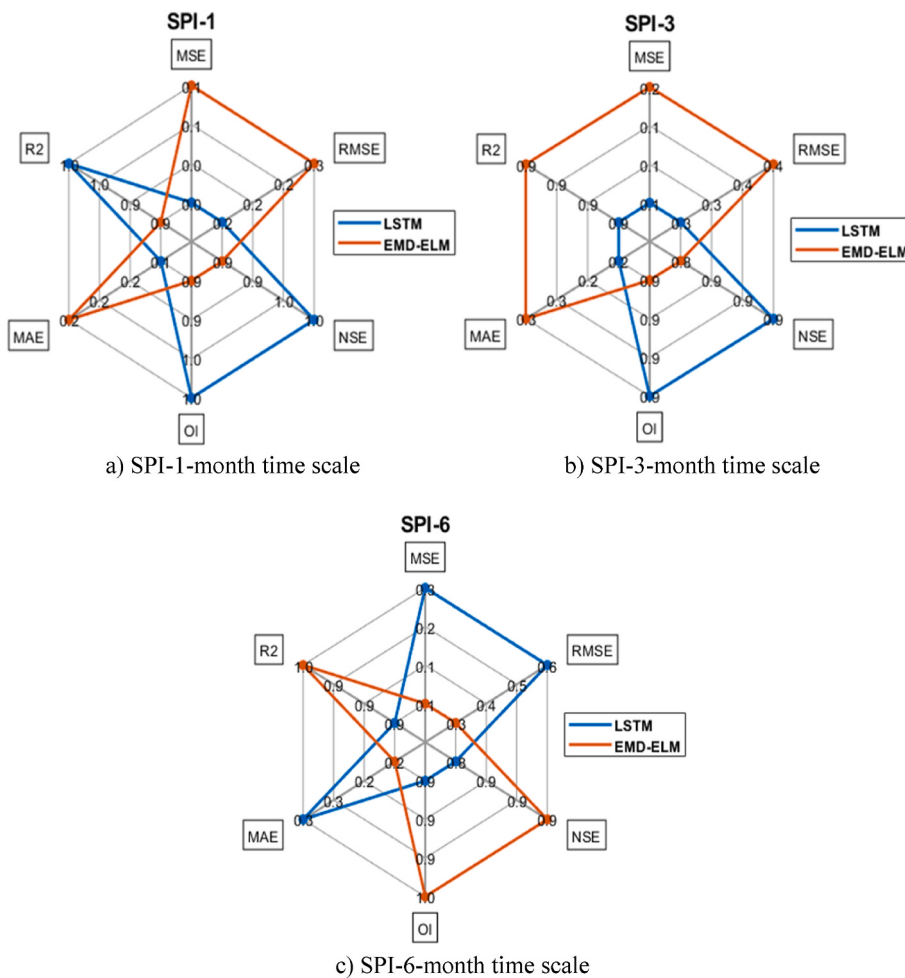


Fig. 11. Radar charts of SPI test results on 1, 3 and 6-month time scales a) SPI-1 b) SPI-3 c) SPI-6-month time scales.

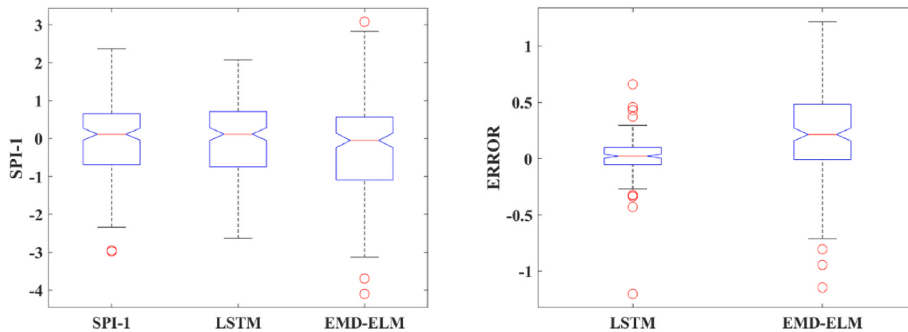


Fig. 12. Boxplot diagram of a) SPI-1-time scale drought, LSTM, and EMD-ELM models b) Error boxplot diagram of the LSTM and EMD-ELM models.

time; no significant correlation was found between the band levels. In other words, the increase or decrease of the band level does not affect the model performance.

- The EMD-ELM hybrid model gave more successful results on the SPI-6-month time scale.
- While the prediction performance of the LSTM model decreased as the time scale increased, the prediction performance of the EMD-ELM hybrid model increased.
- Although the pre-processing technique was not applied, the LSTM model showed superior performance in drought prediction.

- Analyzing the drought time series directly with the LSTM method without pre-processing provides much convenience regarding processing load and time.
- Kruskal-Wallis and ANOVA tests were used to perform a statistical significance test on the analysis outcomes. The EMD-ELM and LSTM models' predictions might represent the mean.
- According to the findings of this research, it is suggested that the LSTM prediction model can be used standalone as a dependable model in drought predictions.

The limitation of this study is that LSTM and ELM methods are used in the SPI drought indexes for Türkiye. In addition, the effectiveness of

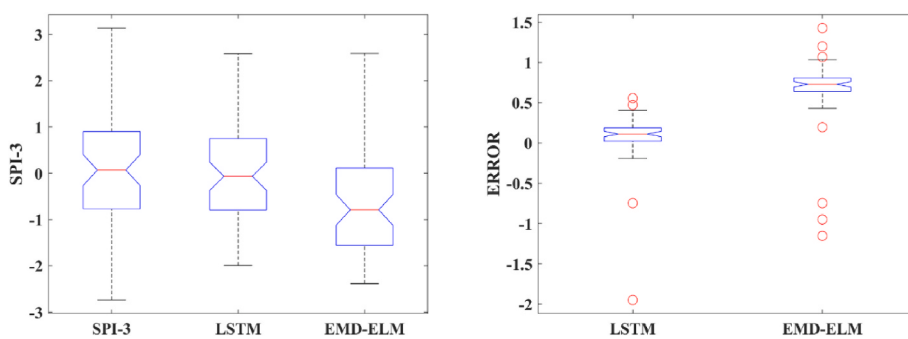


Fig. 13. Boxplot diagram of a) SPI-3- time scale drought, LSTM, and EMD-ELM models b) Error boxplot diagram of the LSTM and EMD-ELM models.

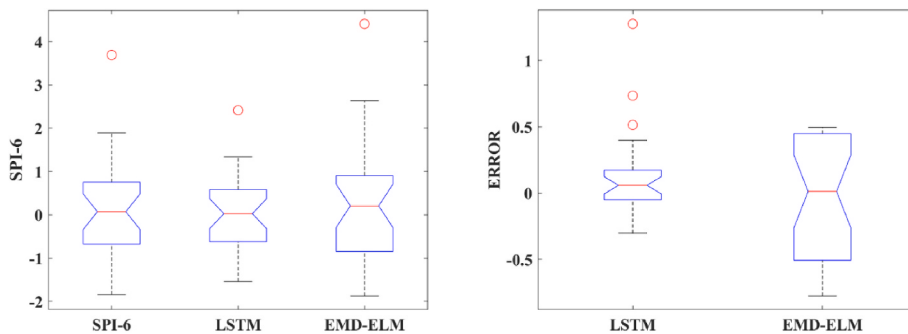


Fig. 14. Boxplot diagram of a) SPI-6- time scale drought, LSTM, and EMD-ELM models b) Error boxplot diagram of the LSTM and EMD-ELM models.

Table 7

ANOVA of the LSTM and EMD-ELM Models in the testing period for SPI-1, SPI-3, and SPI-6-month time scales.

Month Time Scale	Methods	F-statistics	Resultant significance level	H ₀
SPI-1	LSTM	0.04	0.8428	Accept
	EMD-ELM	3.61	0.0584	Accept
SPI-3	LSTM	0.13	0.7242	Accept
	EMD-ELM	10.91	0.0013	Reject
SPI-6	LSTM	0.23	0.6312	Accept
	EMD-ELM	0.04	0.8501	Accept

H₀: $\mu_1 = \mu_2 = \mu_3 = \mu_4$, H₁: $\mu_1 \neq \mu_2 \neq \mu_3 \neq \mu_4$.

Table 8

P-values for the Kruskal-Wallis test at the 95% the confidence level for SPI-1, SPI-3, and SPI-6-month time scales.

Models	Month Time Scale						
		SPI-1		SPI-3		SPI-6	
		p value	H ₀	p value	H ₀	p value	H ₀
LSTM	SPI-1	0.92	Reject	0.60	Reject	0.80	Reject
EMD-ELM	SPI-1	0.07	Reject	0.00	Accept	0.95	Reject

H₀: There are differences between mean predicted and measurement values.

the popular EMD pre-processing method on the machine learning method was researched. It is expected to benefit decision-makers in short-term drought studies for Sakarya, Türkiye. The most important limitation of this study is that the most appropriate band number was investigated in the EMD pretreatment method in previous drought prediction studies, and the number of inputs in machine learning had no effect.

Availability of data and material

Climatic data and hydrometric data provided by The Turkish State Meteorological Service (MGM).

Author contribution

Conceptualization, OC and HC; methodology, OC; data collection, HC; analysis, OC; writing-original draft preparation, OC and HC; writing-review and editing, OC; supervision, OC and HC.

Code availability

The codes were developed from the Matlab website.

Ethics approval

The authors paid attention to the ethical rules in the study. There is no violation of ethics.

Funding

No funds, grants, or other support was received.

Declaration of competing interest

The authors declare that they have no known competing financial interests or personal relationships that could have appeared to influence the work reported in this paper.

Data availability

No data was used for the research described in the article.

Acknowledgement

The authors thank The Turkish State Meteorological Service (MGM)

for the statistics provided.

Abbreviations

$g(x)$	Gamma function's likelihood density function
α	Form parameter
β	Scale parameter
$\Gamma(\alpha)$	Represents the gamma function
x	Precipitation quantity
$H(x)$	Total likelihood distribution
$G(x)$	Total likelihood
q	Probability
t	Time period
f_t	Forgetting process
C_t	Cell state
C_{t-1}	Cell state vector
σ	Sigmoid function
i_t	Sigmoid layer called
x_t	Current input
h_t	Output value of the output gate
h_{t-1}	Latest hidden state
\tilde{C}	New candidate values
O_t	Output gate
MSE	Mean square error
RMSE	Root mean square error
MAE	Mean absolute error
NSE	Nash-Sutcliffe efficiency
OI	Overall index of model performance
R^2	Determination coefficient
N	Number of data sets
\overline{SPI}_{pre}	Averages of predicted
\overline{SPI}_{cal}	Averages of calculated
SPI_{pre}	Prediction values obtained from the models
SPI_{cal}	Drought values calculated
$SPI_{cal\ max}$	Maximum values of the calculated
$SPI_{cal\ min}$	Minimum values of the calculated
W_o, b_o	Trainable variables determined for output gate
W_c, b_c	Trainable variables determined for new candidate values
W_i, b_i	Trainable variables determined for sigmoid layer called
W_f, b_f	Trainable variables determined for first gate
$tanh$	Hyperbolic tangent

References

- Abhirup, D., Biswajeet, P., Alfredo, H., 2020. Spatial Meteorological Drought Forecasting Using Deep Learning for New South Wales, Australia. Abhirup Dikshit. American Geophysical Union, 2020.
- Adib, A., Marashi, S.S., 2019. Meteorological drought monitoring and preparation of long-term and short-term drought zoning maps using regional frequency analysis and L-moment in the Khuzestan province of Iran. *Theor. Appl. Climatol.* 137, 77–87. <https://doi.org/10.1007/s00704-018-2572-8>.
- Adnan, S., Ullah, K., Shuanglin, L., Gao, S., Khan, A.H., Mahmood, R., 2018. Comparison of various drought indices to monitor drought status in Pakistan. *Clim. Dynam.* 51, 1885–1899. <https://doi.org/10.1007/s00382-017-3987-0>.
- Agana, N.A., Homaiifar, A., 2017. A deep learning based approach for long-term drought prediction. In: SoutheastCon 2017. IEEE, pp. 1–8. <https://doi.org/10.1109/SECON.2017.7925314>.
- Akturk, G., Zeybekoglu, U., Yildiz, O., 2022. Assessment of meteorological drought analysis in the kizilirmak river basin, Turkey. *Arabian J. Geosci.* 15 <https://doi.org/10.1007/s12517-022-10119-0>.
- Anshuka, A., van Ogtrop, F.F., Willem Vervoort, R., 2019. Drought forecasting through statistical models using standardised precipitation index: a systematic review and meta-regression analysis. *Nat. Hazards* 97, 955–977. <https://doi.org/10.1007/s11069-019-03665-6>.
- Arslan, O., Bilgil, A., Veske, O., 2016. Standart yağış i?ndisi yöntemi ile kizilirmak havzası'nın meteorolojik kuraklık analizi. Ömer Halisdemir Üniversitesi Mühendislik Bilim. Derg. 5, 188–194. <https://doi.org/10.28948/ngumuh.295572>.
- Başakin, E.E., Ekmekcioğlu, Ö., Çitakoglu, H., Özger, M., 2022. A new insight to the wind speed forecasting: robust multi-stage ensemble soft computing approach based on pre-processing uncertainty assessment. *Neural Comput. Appl.* 34 <https://doi.org/10.1007/s00521-021-06424-6>.
- Bashar, D.A., 2019. Survey on evolving deep learning neural network architectures. *J. Artif. Intell. Capsul. Networks* 2019, 73–82. <https://doi.org/10.36548/jaicn.2019.2.003>.
- Bayram, S., Çitakoglu, H., 2023. Modeling monthly reference evapotranspiration process in Turkey: application of machine learning methods. *Environ. Monit. Assess.* 195 <https://doi.org/10.1007/s10661-022-10662-z>.
- Bayram, S., Ocal, M.E., Laptali Oral, E., Atış, C.D., 2015. Comparison of multi layer perceptron (MLP) and radial basis function (RBF) for construction cost estimation: the case of Turkey. *J. Civ. Engineering Manag.* 22, 480–490. <https://doi.org/10.3846/13923730.2014.897988>.
- Burkov, A., 1997. The Hundred Page Machine Learning, Computer. Quebec City, QC, Canada.
- Citakoglu, H., 2021. Comparison of multiple learning artificial intelligence models for estimation of long-term monthly temperatures in Turkey. *Arabian J. Geosci.* 14 <https://doi.org/10.1007/s12517-021-08484-3>.

- Citakoglu, H., 2015. Comparison of artificial intelligence techniques via empirical equations for prediction of solar radiation. *Comput. Electron. Agric.* 118 <https://doi.org/10.1016/j.compag.2015.08.020>.
- Citakoglu, H., Coşkun, Ö., 2022. Comparison of hybrid machine learning methods for the prediction of short-term meteorological droughts of Sakarya Meteorological Station in Turkey. *Environ. Sci. Pollut. Res.* 29, 75487–75511. <https://doi.org/10.1007/s11356-022-21083-3>.
- Danandeh, M.A., Rikhtehgar, G.A., Mundher, Yaseen, Z., Sorman, A.U., Abualigah, L., 2022. A novel intelligent deep learning predictive model for meteorological drought forecasting. *J. Ambient Intell. Hum. Comput.* 1, 3. <https://doi.org/10.1007/s12652-022-03701-7>.
- Demir, V., 2022. Enhancing monthly lake levels forecasting using heuristic regression techniques with periodicity data component: application of Lake Michigan. *Theor. Appl. Climatol.* 148, 915–929. <https://doi.org/10.1007/s00704-022-03982-0>.
- Demir, V., Citakoglu, H., 2022. Forecasting of solar radiation using different machine learning approaches. *Neural Comput. Appl.*, 0123456789 <https://doi.org/10.1007/s00521-022-07841-x>.
- Demir, V., Yaseen, Z.M., 2022. Neurocomputing Intelligence Models for Lakes Water Level Forecasting: a Comprehensive Review. *Neural Computing and Applications*. Springer London. <https://doi.org/10.1007/s00521-022-07699-z>.
- Docheshmeh, G.A., Alizamir, M., Kisi, O., Elshafie, A., 2022. Drought modelling by standard precipitation index (SPI) in a semi-arid climate using deep learning method: long short-term memory. *Neural Comput. Appl.* 34, 2425–2442. <https://doi.org/10.1007/s00521-021-06505-6>.
- Dogan, S., Berkay, A., Singh, V.P., 2012. Comparison of multi-monthly rainfall-based drought severity indices, with application to semi-arid Konya closed basin, Turkey. *J. Hydrol.* 470–471, 255–268. <https://doi.org/10.1016/j.jhydrol.2012.09.003>.
- Du, J., Liu, Y., Liu, Z., 2018. Study of precipitation forecast based on deep belief networks. *Algorithms* 11, 132. <https://doi.org/10.3390/a11090132>.
- Duvan, A., Aktürk, G., Yıldız, O., 2021. Meteorolojik Kuraklığın Zamansal Ve Alansal Özelliklerine İklim Değişikliğinin Etkisi, Sakarya Havzası Örneği. Mühendislik Bilim. ve Araştırmaları Derg. <https://doi.org/10.46387/bjesr.961816>.
- Edwards, C., McKee, T., Doesken, N., Kleist, J., 1997. Historical analysis of drought in the United States. In: *77th AMS Annual Meeting*. United States.
- Elbeltagi, A., Pande, C.B., Kumar, M., Tolche, A.D., Singh, S.K., Kumar, A., Vishwakarma, D.K., 2023. Prediction of meteorological drought and standardized precipitation index based on the random forest (RF), random tree (RT), and Gaussian process regression (GPR) models. *Environ. Sci. Pollut. Res.* 30, 43183–43202. <https://doi.org/10.1007/s11356-023-25221-3>.
- Erinc, S., 1965. *A Trial on Rainfall Effectiveness*. Bahá Press, İstanbul.
- Fadaei-Kermani, E., Ghaeini-Hessarooyeh, M., 2020. Fuzzy nearest neighbor approach for drought monitoring and assessment. *Appl. Water Sci.* 10, 130. <https://doi.org/10.1007/s13201-020-01212-4>.
- Fan, H., Jiang, M., Xu, L., Zhu, H., Cheng, J., Jiang, J., 2020. Comparison of long short term memory networks and the hydrological model in runoff simulation. *Water* 12, 2–15. <https://doi.org/10.3390/w12010175>.
- Fung, K.F., Huang, Y.F., Koo, C.H., Soh, Y.W., 2020. Drought forecasting: a review of modelling approaches 2007–2017. *J. Water Clim. Chang.* 11, 771–799. <https://doi.org/10.2166/wcc.2019.236>.
- Ghasemi, M.M., Mokarram, M., Zarei, A.R., 2022. Assessing the performance of SN-SPI and SPI and the trend assessment of drought using the XI correlation technique over Iran. *J. Water Clim. Chang.* 13, 3152–3169. <https://doi.org/10.2166/wcc.2022.176>.
- Gholizadeh, R., Hasan, Yılmaz, Mehr, A.D., 2022. Multitemporal meteorological drought forecasting using Bat-ELM. *Acta Geophys.* 1, 3. <https://doi.org/10.1007/s11600-022-00739-1>.
- Ham, Y.-S., Sonu, K.-B., Paek, U.-S., Om, K.-C., Jong, S.-I., Jo, K.-R., 2022. Comparison of LSTM network, neural network and support vector regression coupled with wavelet decomposition for drought forecasting in the western area of the DPRK. *Nat. Hazards*. <https://doi.org/10.1007/s11069-022-05781-2>.
- Hochreiter, S., Schmidhuber, J., 1997. Long short-term memory. *Neural Comput.* 9, 1735–1780. <https://doi.org/10.1162/neco.1997.9.8.1735>.
- Huang, G.-B., Zhu, Q.-Y., Siew, C.-K., 2006. Extreme learning machine: theory and applications. *Neurocomputing* 70, 489–501. <https://doi.org/10.1016/j.neucom.2005.12.126>.
- Huang, N.E., Shen, Z., Long, S.R., Wu, M.C., Shih, H.H., Zheng, Q., Yen, N.-C., Tung, C.C., Liu, H.H., 1998. The empirical mode decomposition and the Hilbert spectrum for nonlinear and non-stationary time series analysis. *Proc. R. Soc. London. Ser. A. Math. Phys. Eng. Sci.* 454, 903–995. <https://doi.org/10.1098/rspa.1998.0193>.
- Ju, X., Yang, X., Chen, L., Wang, Y., 1997. Research on determination of station indexes and division of regional flood/drought grades in China. *J. Appl. Meteorol. Sci.* 8, 26–33.
- Katipoğlu, O.M., 2023. Prediction of streamflow drought index for short-term hydrological drought in the semi-arid yesilirmak basin using wavelet transform and artificial intelligence techniques. *Sustainability* 15, 1109. <https://doi.org/10.3390/su15021109>.
- Kisi, O., Demir, V., Kim, S., 2017. Estimation of long-term monthly temperatures by three different adaptive neuro-fuzzy approaches using geographical inputs. *J. Irrigat. Drain. Eng.* 143, 04017052 [https://doi.org/10.1061/\(ASCE\)IR.1943-4774.0001242](https://doi.org/10.1061/(ASCE)IR.1943-4774.0001242).
- Latifoglu, L., 2022a. A novel combined model for prediction of daily precipitation data using instantaneous frequency feature and bidirectional long short time memory networks. *Environ. Sci. Pollut. Res.* 29, 42899–42912. <https://doi.org/10.1007/s11356-022-18874-z>.
- Latifoglu, L., 2022b. The performance analysis of robust local mean mode decomposition method for forecasting of hydrological time series. *Iran. J. Sci. Technol. Trans. Civ. Eng.* 46, 3453–3472. <https://doi.org/10.1007/s40996-021-00809-2>.
- Latifoglu, L., 2022c. Application of the novel circulant singular spectrum analysis ensemble model for forecasting of streamflow data. *Arabian J. Geosci.* 15 <https://doi.org/10.1007/s12517-022-10230-2>.
- LeCun, Y., Bengio, Y., Hinton, G., 2015. Deep learning. *Nature* 521, 436–444. <https://doi.org/10.1038/nature14539>.
- Lei, Y., Lin, J., He, Z., Zuo, M.J., 2013. A review on empirical mode decomposition in fault diagnosis of rotating machinery. *Mech. Syst. Signal Process.* 35, 108–126. <https://doi.org/10.1016/j.ymssp.2012.09.015>.
- Li, G., Ma, X., Yang, H., 2018. A hybrid model for monthly precipitation time series forecasting based on variational mode decomposition with extreme learning machine. *Information* 9, 177. <https://doi.org/10.3390/info9070177>.
- Li, T., Wu, T., Liu, Z., 2020. Nonlinear unsteady bridge aerodynamics: reduced-order modeling based on deep LSTM networks. *J. Wind Eng. Ind. Aerod.* 198, 104116. <https://doi.org/10.1016/j.jweia.2020.104116>.
- Lian, Cheng, Zeng, Z., Yao, Wei, Tang, Huiming, Lian, C., Zeng, Á.Z., Yao, W., Tang, H., 2013. Displacement prediction model of landslide based on a modified ensemble empirical mode decomposition and extreme learning machine. *Nat. Hazards* 66, 759–771. <https://doi.org/10.1007/s11069-012-0517-6>.
- Lloyd-Hughes, B., Saunders, M.A., 2002. A drought climatology for Europe. *Int. J. Climatol.* 22, 1571–1592. <https://doi.org/10.1002/joc.846>.
- Lotfifrad, M., Esmaeili-Gisavandani, H., Adib, A., 2022. Drought monitoring and prediction using SPI, SPEI, and random forest model in various climates of Iran. *J. Water Clim. Chang.* 13, 383–406. <https://doi.org/10.2166/wcc.2021.287>.
- Lu, C.-J., Shao, Y.E., 2012. Forecasting computer products sales by integrating ensemble empirical mode decomposition and extreme learning machine. *Math. Probl. Eng.* 15 <https://doi.org/10.1155/2012/831201>, 2012.
- McKee, T.B., N.J., Kleist, J., 1993. The relationship of drought frequency and duration to time scales. Anaheim, California, 179–184, in: *Eighth Conference on Applied Climatology*. CA: In: Proc. 8th Conf. On Applied Climatology. American Meteorological Society, Boston, pp. 17–22.
- Mokhtar, A., Jalali, M., He, H., Al-Ansari, N., Elbeltagi, A., Alsafadi, K., Abdo, H.G., Sammen, S.S., Gaysi-Agyei, Y., Rodrigo-Comino, J., 2021. Estimation of SPEI meteorological drought using machine learning algorithms. *IEEE Access* 9, 65503–65523. <https://doi.org/10.1109/ACCESS.2021.3074305>.
- Nalbantis, I., Tsakiris, G., 2009. Assessment of hydrological drought revisited. *Water Resour. Manag.* 23, 881–897. <https://doi.org/10.1007/s11269-008-9305-1>.
- Nash, J.E., Sutcliffe, J.V., 1970. River flow forecasting through conceptual models part I — a discussion of principles. *J. Hydrol.* 10, 282–290. [https://doi.org/10.1016/0022-1694\(70\)90255-6](https://doi.org/10.1016/0022-1694(70)90255-6).
- Olah, C., 2015. Understanding lstm networks [WWW Document]. <http://colah.github.io/posts/2015-08-Understanding-LSTMs/>.
- Özbayrak, A., Ali, M.K., Çitakoglu, H., 2023. Buckling load estimation using multiple linear regression analysis and multigene genetic programming method in cantilever beams with transverse stiffeners. *Arabian J. Sci. Eng.* 48, 5347–5370. <https://doi.org/10.1007/s13369-022-07445-6>.
- Özger, M., Başakan, E.E., Ekmekcioğlu, Ö., Hacısüleyman, V., 2020. Comparison of wavelet and empirical mode decomposition hybrid models in drought prediction. *Comput. Electron. Agric.* 179, 105851 <https://doi.org/10.1016/j.compag.2020.105851>.
- Palmer, W.C., 1965. *Meteorological Drought*. U.S. Weather Bureau, Res. Pap., Weather Bureau, Washington, DC. No. 45.
- Pande, C.B., Al-Ansari, N., Kushwaha, N.L., Srivastava, A., Noor, R., Kumar, M., Moharir, K.N., Elbeltagi, A., 2022. Forecasting of SPI and meteorological drought based on the artificial neural network and M5P model tree. *Land* 11, 2040. <https://doi.org/10.3390/land1112040>.
- Pande, C.B., Costache, R., Sammen, S.S., Noor, R., Elbeltagi, A., 2023a. Combination of data-driven models and best subset regression for predicting the standardized precipitation index (SPI) at the Upper Godavari Basin in India. *Theor. Appl. Climatol.* 152, 535–558. <https://doi.org/10.1007/s00704-023-04426-z>.
- Pande, C.B., Kushwaha, N.L., Orimoloye, I.R., Kumar, R., Abdo, H.G., Tolche, A.D., Elbeltagi, A., 2023b. Comparative assessment of improved SVM method under different kernel functions for predicting multi-scale drought index. *Water Resour. Manag.* 37, 1367–1399. <https://doi.org/10.1007/s11269-023-03440-0>.
- Poornima, S., Pushpalatha, M., 2019. Drought prediction based on SPI and SPEI with varying timescales using LSTM recurrent neural network. *Soft Comput.* 23, 8399–8412. <https://doi.org/10.1007/s00500-019-04120-1>.
- Press, W., 2007. *Numerical recipes*. In: *The Art of Scientific Computing*, third ed. Cambridge University Press, Cambridge.
- Republic of Turkey, Ministry of Agriculture and Forestry General Directorate of Meteorology. <https://mgm.gov.tr/veridegerlendirme/il-ve-ilceler-istatistik.aspx>. Access date: March 2022.
- Sahani, M., Dash, P.K., Samal, D., 2020. A real-time power quality events recognition using variational mode decomposition and online-sequential extreme learning machine. *Measurement* 157, 107597. <https://doi.org/10.1016/j.measurement.2020.107597>.
- Sattari, M.T., Apaydin, H., Band, S.S., Mosavi, A., Prasad, R., 2021. Comparative analysis of kernel-based versus ANN and deep learning methods in monthly reference evapotranspiration estimation. *Hydrool. Earth Syst. Sci.* 25, 603–618. <https://doi.org/10.5194/hess-25-603-2021>.
- Seo, Y., Kwon, S., Choi, Y., 2018. Short-term water demand forecasting model combining variational mode decomposition and extreme learning machine. *Hydrology* 5, 54. <https://doi.org/10.3390/hydrology5040054>.
- Shaowei, Z., Hongchao, Z., Pengcheng, R., Guangjie, X., Bangdong, L., Wencheng, D., Liying, W., 2013. Application of standardized precipitation evapotranspiration index in China. *Clim. Environ. Res.* 18, 617–625.

- Shukla, S., Wood, A.W., 2008. Use of a standardized runoff index for characterizing hydrologic drought. *Geophys. Res. Lett.* 35 <https://doi.org/10.1029/2007GL032487>.
- Sirdas, S., 2002. *Meteorological Drought Modelling and Application to Turkey*. Istanbul Technical University, Graduate School of Science Engineering and Technology, Istanbul.
- Sırdaş, S., Sen, Z., 2003. Spatio-temporal drought analysis in the Trakya region, Turkey. *Hydrol. Sci. J.* 48, 809–820. <https://doi.org/10.1623/hysj.48.5.809.51458>.
- Tigkas, D., Vangelis, H., Tsakiris, G., 2015. DrinC: a software for drought analysis based on drought indices. *Earth Sci. Informatics* 8, 697–709. <https://doi.org/10.1007/s12145-014-0178-y>.
- Tsakiris, G., Vangelis, H., 2005. Establishing a drought index incorporating evapotranspiration. *Eur. water* 9, 3–11.
- Vicente-Serrano, S.M., Beguería, S., López-Moreno, J.I., 2010. A multiscalar drought index sensitive to global warming: the standardized precipitation evapotranspiration index. *J. Clim.* 23, 1696–1718. <https://doi.org/10.1175/2009JCLI2909.1>.
- Wang, J., Lu, S., Wang, S.-H., Zhang, Y.-D., 2022. A review on extreme learning machine. *Multimed. Tool. Appl.* 1 <https://doi.org/10.1007/s11042-021-11007-7>.
- Wu, X., Zhou, J., Yu, H., Liu, D., Xie, K., Chen, Y., Hu, J., Sun, H., Xing, F., 2021. The development of a hybrid wavelet-ARIMA-LSTM model for precipitation amounts and drought analysis. *Atmosphere* 12, 74. <https://doi.org/10.3390/atmos12010074>.
- Yang, H.-F., Chen, Y.-P.P., 2019. Representation learning with extreme learning machines and empirical mode decomposition for wind speed forecasting methods. *Artif. Intell.* 277, 103176 <https://doi.org/10.1016/j.artint.2019.103176>.
- Yasir, M., Koh, B.-H., 2018. Data decomposition techniques with multi-scale permutation entropy calculations for bearing fault diagnosis. *Sensors* 18, 1278. <https://doi.org/10.3390/s18041278>.
- Zarei, A.R., 2019. Analysis of changes trend in spatial and temporal pattern of drought over south of Iran using standardized precipitation index (SPI). *SN Appl. Sci.* 1, 465. <https://doi.org/10.1007/s42452-019-0498-0>.
- Zarei, A.R., Mahmoudi, M.R., 2021. Assessing the influence of PET calculation method on the characteristics of UNEP aridity index under different climatic conditions throughout Iran. *Pure Appl. Geophys.* 178, 3179–3205. <https://doi.org/10.1007/s00024-021-02786-z>.
- Zeybekoglu, U., Aktürk, G., 2021. A comparison of the China-Z index (CZI) and the standardized precipitation index (SPI) for drought assessment in the hirfanlı dam basin in central Turkey. *Arabian J. Geosci.* 14 <https://doi.org/10.1007/S12517-021-09095-8>.
- Zhai, L., Feng, Q., 2009. Spatial and temporal pattern of precipitation and drought in Gansu Province, Northwest China. *Nat. Hazards* 49, 1–24. <https://doi.org/10.1007/s11069-008-9274-y>.
- Zhang, X., Zhao, D., Wang, T., Wu, X., Duan, B., 2022. A novel rainfall prediction model based on CEEMDAN-PSO-ELM coupled model. *Water Supply*. <https://doi.org/10.2166/ws.2022.115>.
- Zhao, J., Mao, X., Chen, L., 2019. Speech emotion recognition using deep 1D & 2D CNN LSTM networks. *Biomed. Signal Process Control* 47, 312–323. <https://doi.org/10.1016/j.bspc.2018.08.035>.